Brigham Young University
Department of Electrical and
Computer Engineering

459 Clyde Building
Provo, Utah 84602

Refinement of SIRF for SASS

Quinn P. Remund

8 June 1998

MERS Technical Report # MERS 98-04
ECEN Department Report # TR-L104-98.4

Microwave Earth Remote Sensing (MERS) Laboratory

Refinement of SIRF for SASS

Quinn P. Remund
Brigham Young University

June 8, 1998

Abstract

The utility of scatterometer data is increased by the scatterometer image reconstruction with filter (SIRF) algorithm. This method uses several passes of the satellite to effectively enhance the spatial resolution of the data. Three parameters of SIRF influence its ability to converge to the true values and must be tuned when SIRF is applied to data from different instruments. Initialization values, number of iterations, and $\mathcal{B}$ update weighting all affect the performance of SIRF. Originally developed for Seasat-A scatterometer (SASS) data, the algorithm was refined for NSCAT and ERS-1/2 AMI scatterometers. With the new knowledge gained from these studies, this report addresses the refinement of SIRF across the three parameters for SASS data. Synthetic truth images are constructed. SASS measurement data is simulated using actual SASS data in conjunction with the truth images. The convergence properties of SIRF are examined using several statistical measures of error and correlation. The results indicate that initialization values of $\mathcal{A}_{init}$=-8.4 dB and $\mathcal{B}_{init}$=-0.14 dB/deg, 50 iterations, and b_{acc} values of 15 to 20 should be used.

1 Introduction

Remote sensing of the earth's surface from space has proven invaluable in many scientific disciplines. In particular, scatterometers such as the Seasat-A Scatterometer System (SASS) and the NASA Scatterometer (NSCAT) are sensitive to surface parameters. However, the low resolution of these instruments has limited their utility. Recently a new method called the scatterometer image reconstruction with filter (SIRF) algorithm has been developed to increase the resolution of the data by using multiple passes of the satellite over a target region [1]. SIRF is basically a bivariate, nonlinear version of the multiplicative algebraic reconstruction technique. This method produces a maximum entropy solution which is desirable for edge reconstruction in the imagery.

For a limited range of incidence angles, σ^o is approximately a linear function of θ,

$$10\log_{10}\sigma^o(\theta) = \mathcal{A} + \mathcal{B}(\theta - 40^\circ) \qquad (1)$$

where $\mathcal{A}$ and $\mathcal{B}$ are functions of surface characteristics, azimuth angle, and polarization. $\mathcal{A}$ is the σ^o value at 40° incidence and $\mathcal{B}$ describes the dependence of σ^o on θ. $\mathcal{A}$ and $\mathcal{B}$ provide valuable information about the surface. SIRF produces images of both $\mathcal{A}$ and $\mathcal{B}$.

Several parameters in the SIRF algorithm affect its convergence characteristics. The number of iterations, initialization values, and B weighting all influence the performance of SIRF. The iteration parameter determines how long SIRF iterates to achieve a final estimate of the image. Initialization values for both $\mathcal{A}$ and $\mathcal{B}$ are used to give SIRF a starting estimate of $\mathcal{A}$ and $\mathcal{B}$. The SIRF algorithm contains heavy update damping to avoid noise amplification. This works well in high noise scenarios, but may limit the ability of the algorithm to converge to the true values in a reasonable number of iterations when noise levels are lower. For this reason, the $\mathcal{B}$ updates are often weighted by a factor (b_{acc}) to accelerate the convergence of SIRF. The original SASS SIRF uses b_{acc}=1.

The algorithm was optimized for NSCAT across all of these parameters by observing the error and correlation statistics of simulated SIRF images and their ground truth counterparts [2]. One of the conclusions of this study was to use the global average $\mathcal{A}$ and $\mathcal{B}$ values for the initialization. This was chosen to minimize expected convergence time. Since NSCAT (13.995 GHz) and SASS (14.6 GHz) are both Ku-band instruments, the surface responses should be very similar. For this reason, the same initialization values are used for SASS as for NSCAT, namely $\mathcal{A}$=-8.4 dB and $\mathcal{B}$=-0.14 dB/deg.

This report describes a study that refines SIRF for SASS data by adjusting the iteration and $\mathcal{B}$ weighting parameters. Section 2 discusses the generation of simulated SASS imagery. Section 3 describes the statistical analysis of these images as compared with the truth images. In section 4, the conclusions of the study are given.

2 Generating Simulation Data

To examine the effects of the SIRF parameters, synthetic $\mathcal{A}$ and $\mathcal{B}$ truth images are created. The images are created at higher resolution (4.45 km per pixel) than the nominal resolution of the satellite (25 km) with dimensions of approximately $8^\circ \times 8^\circ$. The images use a rectangular latitude/longitude projection. Two simulations are performed using the data. The first has homogeneous constant truth values $\mathcal{A}$=-10.0 and $\mathcal{B}$=-0.1. The second is a heterogeneous image that illustrates features that are similar to those seen in real scatterometer imagery. Figure 1 shows the four truth images used in this study.

SASS L1.5 data records contain geolocation, azimuth angle, incidence angle, and σ^o information for each measurement cell. Simulated data is generated using 60 days of actual SASS data (1978 JD 188-248) taken from the Amazon Basin (latitude range of 0.0°S to 8.0°S, longitude range of 55.0°W to 63.0°W) combined with the truth images. The actual data provides geolocation and incidence angle information and the truth images are used to create synthetic σ^o values. σ^o is computed from effective $\mathcal{A}$ and $\mathcal{B}$ values in the measurement footprint (see Figure 2),

$$A_{eff} = \sum_{c=L_k}^{R_k} \sum_{a=B_k}^{T_k} h(x,y;k) A_{truth}(x,y;k) \tag{2}$$

$$B_{eff} = \sum_{c=L_k}^{R_k} \sum_{a=B_k}^{T_k} h(x,y;k) B_{truth}(x,y;k) \tag{3}$$

where L_k, R_k, T_k, and B_k define a bounding rectangle for the k^{th} hexagonal σ^o measurement cell, $h(x,y;k)$ is the weighting function for the $(x,y)^{th}$ resolution element

($h(x, y; k)$=0 or 1 for NSCAT), $A_{truth}(x, y; k)$ is the $\mathcal{A}$ value for the $(x, y)^{th}$ resolution element, and $B_{truth}(x, y; k)$ is the corresponding $\mathcal{B}$ value. The noiseless σ^o then becomes

$$\sigma^o_{nl} = A_{eff} + B_{eff}(\theta - 40^\circ). \tag{4}$$

Realistic noise is added to σ^o_{nl} by using theoretical values of the noise variance. The simulated σ^o is given by

$$\sigma^o = \sigma^o_{nl}(1 + k_p \nu) \tag{5}$$

where and ν is a zero-mean Gaussian random variable with unity variance. Since no SASS K_p data was available, typical NSCAT K_p values were observed. Figure 3 shows histograms of K_p for several diverse regions throughout the earth. This figure shows that K_p rarely exceeds 0.10. Assuming that SASS σ^o measurements are at most twice as noisy as NSCAT, four values are used: K_p=0.0 (noiseless), K_p=0.05, K_p=0.10, K_p=0.15, and K_p=0.20. Each of these values is used in simulation for both ground truth scenes.

3 Statistical Analysis of Simulated Images

SIRF was run using the simulated data for all ground truths and all of the selected K_p levels. At each iteration, the resulting reconstructed image was compared with the truth image. A simple statistical analysis was performed to provide metrics for the performance of SIRF in all the test scenarios. Several statistical measures were used. In the constant truth simulation, the mean as well as the standard deviation were used to monitor convergence to the true $\mathcal{A}$ and $\mathcal{B}$ values. For the heterogeneous case, the mean error, error standard deviation, RMS error, and the correlation coefficient were used. Each of these provide information about the ability of SIRF to reconstruct the true image as a function of iteration number (N) and b_{acc}.

3.1 Constant Truth

For the constant truth simulation, the initialization values used were $\mathcal{A}_{init}$=-20.0 and $\mathcal{B}_{init}$=–0.2 to simulate a near worst case situation where the algorithm had a significant distance to converge. The means and standard deviations were computed after each iteration for all K_p values. The results are plotted in Figures 4-13.

Figures 4-5 illustrate the noiseless simulation results. The $\mathcal{A}$ values converge to the true value by the 25th iteration regardless of the b_{acc} value although the b_{acc}=1 plot is biased a little high. The $\mathcal{A}$ standard deviation shows the noise level in the reconstructed image. This metric converges to a final low value. Higher b_{acc} means quicker noise level reduction. The effects of $\mathcal{B}$ update weighting are more pronounced in the $\mathcal{B}$ error plots. Without $\mathcal{B}$ acceleration, SIRF was unable to converge to the true value even after 50 iterations. Again, higher b_{acc} means quicker convergence and lower noise level.

As K_p rises, some interesting things begin to happen. First, we observe that regardless of K_p level, the $\mathcal{A}$ mean seems to converge in a very similar manner. The $\mathcal{A}$ error noise level has an increasing noise floor as K_p increases. When K_p=0.05, the standard deviation appears to converge to this noise floor. However, for higher K_p's the noise in the image is amplified at each iteration diverging from the theoretical floor. For the $\mathcal{A}$ statistics, more $\mathcal{B}$ weighting yields better results. While $\mathcal{B}$ weighting enhances the ability to reconstruct the images according to the $\mathcal{A}$ constant truth statistics, the noise amplification indicates that iterations may need to be limited.

Like $\mathcal{A}$, the $\mathcal{B}$ mean converges in a similar manner across all observed values of K_p. Again, more b_{acc} results in quicker convergence. The $\mathcal{B}$ standard deviation converges to higher and higher noise floors as K_p is increased. In contrast to the $\mathcal{A}$ standard deviation, the $\mathcal{B}$ noise level does not increase significantly with iteration number. Also, in noisy scenarios (k_p >0.05) $\mathcal{B}$ standard deviation is an increasing function of b_{acc}. While the $\mathcal{A}$ statistics provide an argument for using arbitrarily high b_{acc}, the $\mathcal{B}$ statistics indicate that excessively high b_{acc} may degrade the quality of the final $\mathcal{B}$ image.

3.2 Heterogeneous Truth

The heterogeneous truth simulation provides a feel for the performance of SIRF on actual SASS data since features in the truth image are similar to features that may actually be observed. For these simulations, the NSCAT optimized initialization values of $\mathcal{A}_{init}$=-8.4 and $\mathcal{B}_{init}$=-0.14 are used. Several statistics were computed at after each iteration: mean error, error standard deviation, RMS error, and correlation coefficient. Figures 14-23 show these statistics as a function of iteration for all of the K_p values.

The $\mathcal{A}$ plots show that when b_{acc} is greater than about 10, all statistics converge to the same value. The b_{acc}=1 curves are biased to slightly poorer values. Hence, at least b_{acc}=10 is desirable. Also, all of the statistics continue to improve with iteration number (at least up to 50 iterations) for $k_p \leq 0.15$. When the extreme case of K_p =0.20 is encountered, each statistic improves for a time, then begins to degrade. However, the level of degradation is not very significant. For correlation coefficient, the maximum value is 0.9145 and the value after 50 iterations is 0.9122.

It is clear from the $\mathcal{B}$ plots that some $\mathcal{B}$ weighting is definitely needed since b_{acc}=1 has the poorest statistics for all K_p. When $k_p \leq 0.10$ we find that more $\mathcal{B}$ update weighting results in lower error and higher correlation. After 30 iterations, all $b_{acc} \geq 20$ yield very similar results for these noise levels. In contrast when K_p rises above 0.10, b_{acc}=10 gives the best results and b_{acc}=50 the poorest. This suggests that for excessively noisy measurements, too much $\mathcal{B}$ update weighting can amplify the noise and degrade the images.

A visual analysis of the reconstruction properties of SIRF for SASS data can be obtained by observing Figures 24-29. Figures 24-25 illustrate the $\mathcal{A}$ and $\mathcal{B}$ images as a function of iteration number and b_{acc} with K_p fixed at 0.10. Figures 26-27 show the images at different K_p and b_{acc} values with iteration number set at 50. Finally, Figures 28-29 display the images over several K_p and iteration number values for b_{acc} fixed at 30.

4 Conclusion

The SIRF algorithm is an effective tool in enhancing the resolution of SASS radar imagery. Several parameters influence its ability to properly estimate the original image. Initialization values, number of iterations, and $\mathcal{B}$ update weighting all influence the convergence characteristics of SIRF. The initialization values are chosen to be the same as those used for NSCAT since both are Ku-band instruments, namely $\mathcal{A}_{init}$=-8.4 and

$\mathcal{B}_{init}$=-0.14. Iteration number is also chosen to be the same as NSCAT since the correlation coefficient and error statistics continue to improve even at the 50th iteration for most cases. The only exception is when K_p=0.20. At this noise level the correlation coefficient reaches a maximum then decreases, but only slightly.

The major parameter in need of tuning for SASS is the $\mathcal{B}$ update weighting (b_{acc}). It is not clear that the SASS measurement noise is the same as for NSCAT. For this reason, this study used values that were more than twice as big as typical NSCAT K_p values. The simulations showed that there is a definite need to accelerate the $\mathcal{B}$ updates regardless of noise level since the b_{acc}=1 simulation did not converge to the correct $\mathcal{A}$ or $\mathcal{B}$ values after 50 iterations. For the $\mathcal{A}$ images, increasing b_{acc} only improves the statistics to a certain point. For example, if $b_{acc}\geq$ 10 is used, the $\mathcal{A}$ error and correlation statistics are very similar. However, the $\mathcal{B}$ statistics tell a different story. When K_p is low all $b_{acc}\geq$ 20 give similar results. In contrast, when $k_p \geq 0.15$, more $\mathcal{B}$ update weighting means lower correlation coefficient. For this reason, it is recommended that an intermediate b_{acc}=15 to 20 be used to balance this trade-off.

References

[1] D. Long, P. Hardin, and P. Whiting, "Resolution Enhancement of Spaceborne Scatterometer Data," *IEEE Transactions on Geoscience and Remote Sensing*, vol. 31, pp. 700–715, 1993.

[2] Q. Remund and D. Long, "Optimization of SIRF for NSCAT," *BYU MERS Technical Report*, no. 97-03, July 1997.

5 Figures

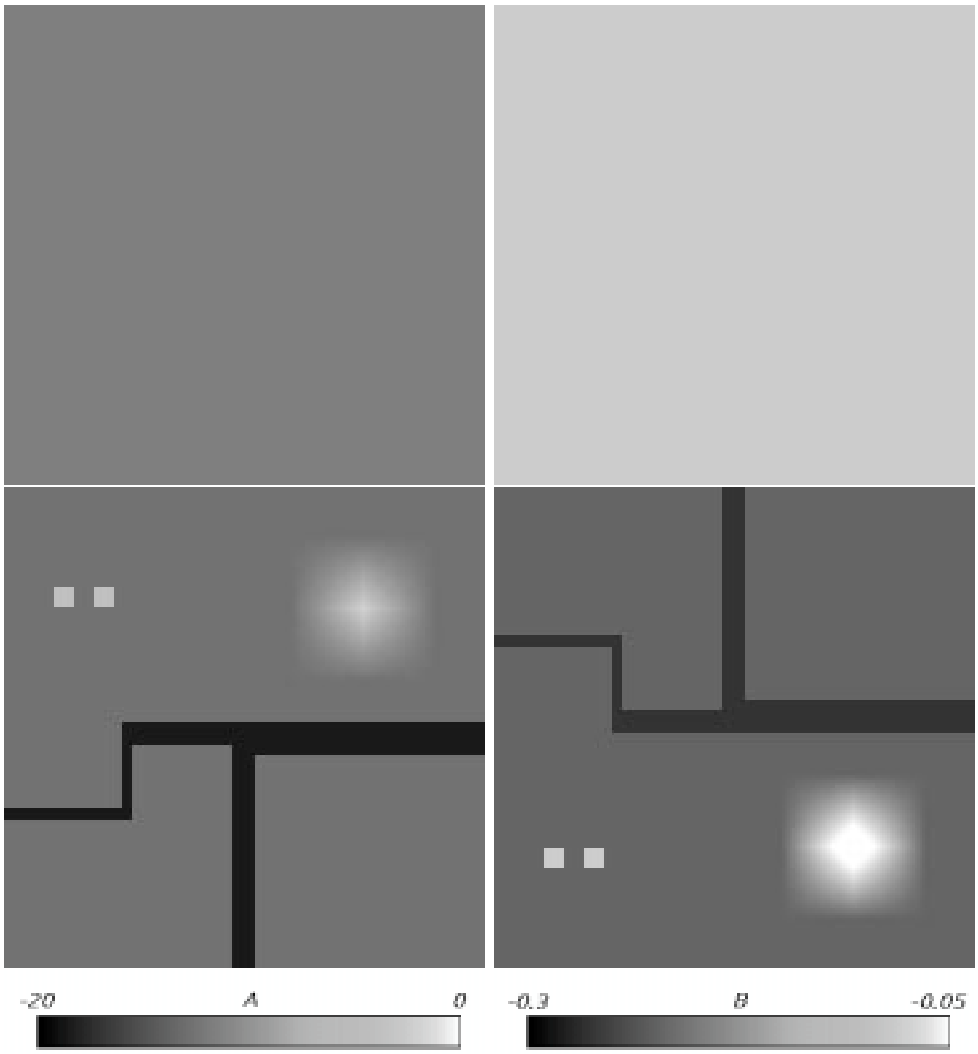

Figure 1: Truth images used in the SASS SIRF simulations. Top left: constant $\mathcal{A}$ image ($\mathcal{A}$= -10.0 dB). Top right: constant $\mathcal{B}$ image ($\mathcal{B}$= -0.1 dB/deg). Lower left: heterogeneous $\mathcal{A}$ image. Lower right: heterogeneous $\mathcal{B}$ image.

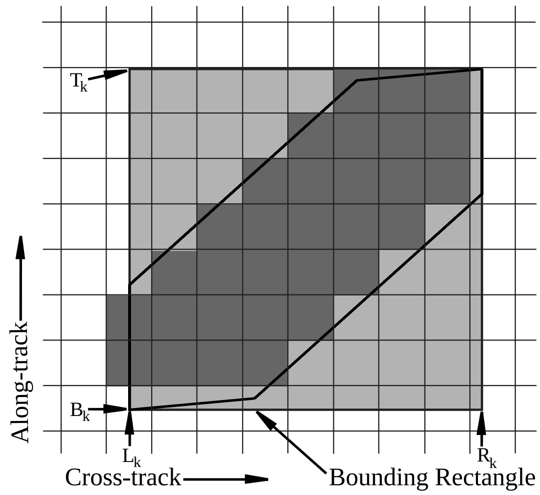

Figure 2: An integrated NSCAT σ^o cell overlaying the high resolution grid. Only the shaded square grid elements have nonzero $h_{(x,y)}$. The bounding rectangle is also indicated.

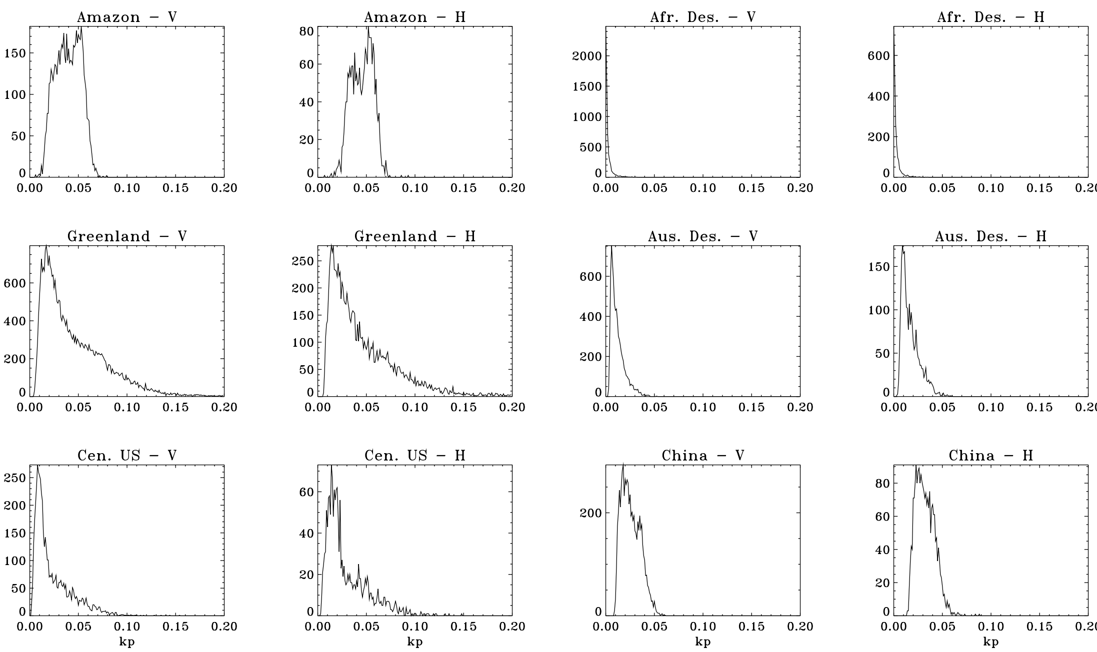

Figure 3: Histograms of K_p for several sample regions over the earth. For each region, both V-pol and H-pol measurements are represented.

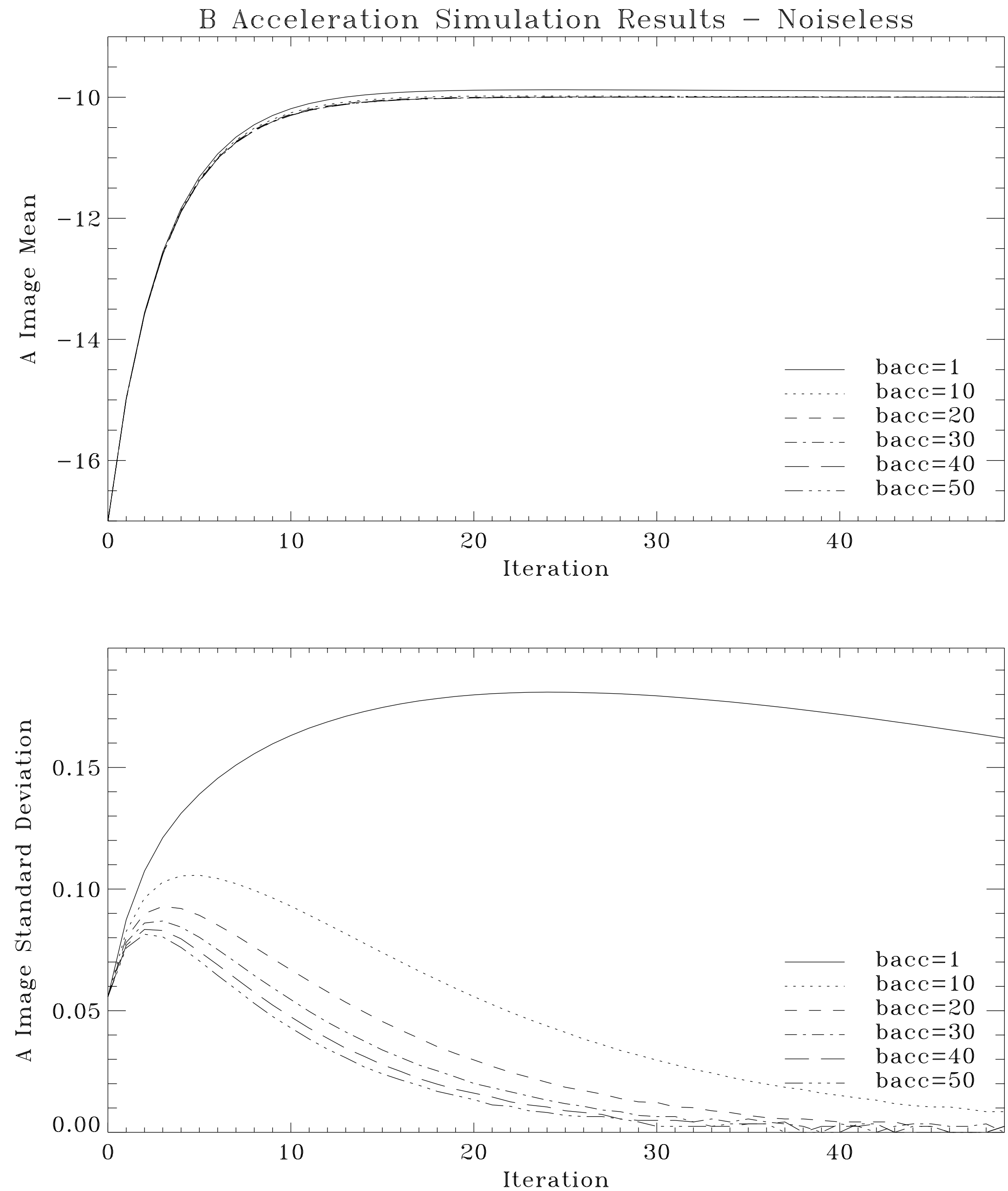

Figure 4: Simulated SIRF $\mathcal{A}$ mean and standard deviations as a function of iteration number and b_{acc} for K_p=0.0.

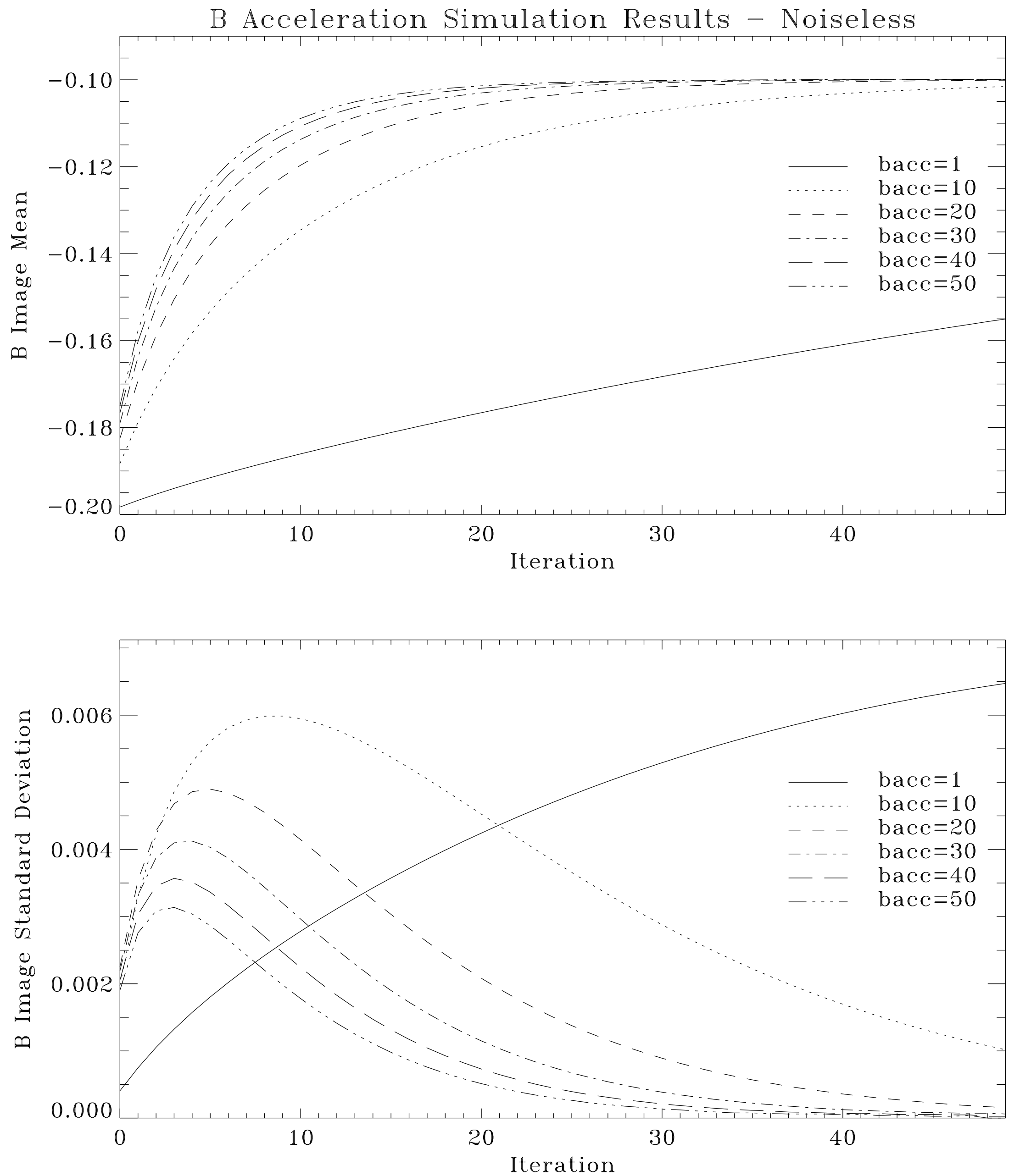

Figure 5: Simulated SIRF $\mathcal{B}$ mean and standard deviations as a function of iteration number and b_{acc} for K_p=0.0.

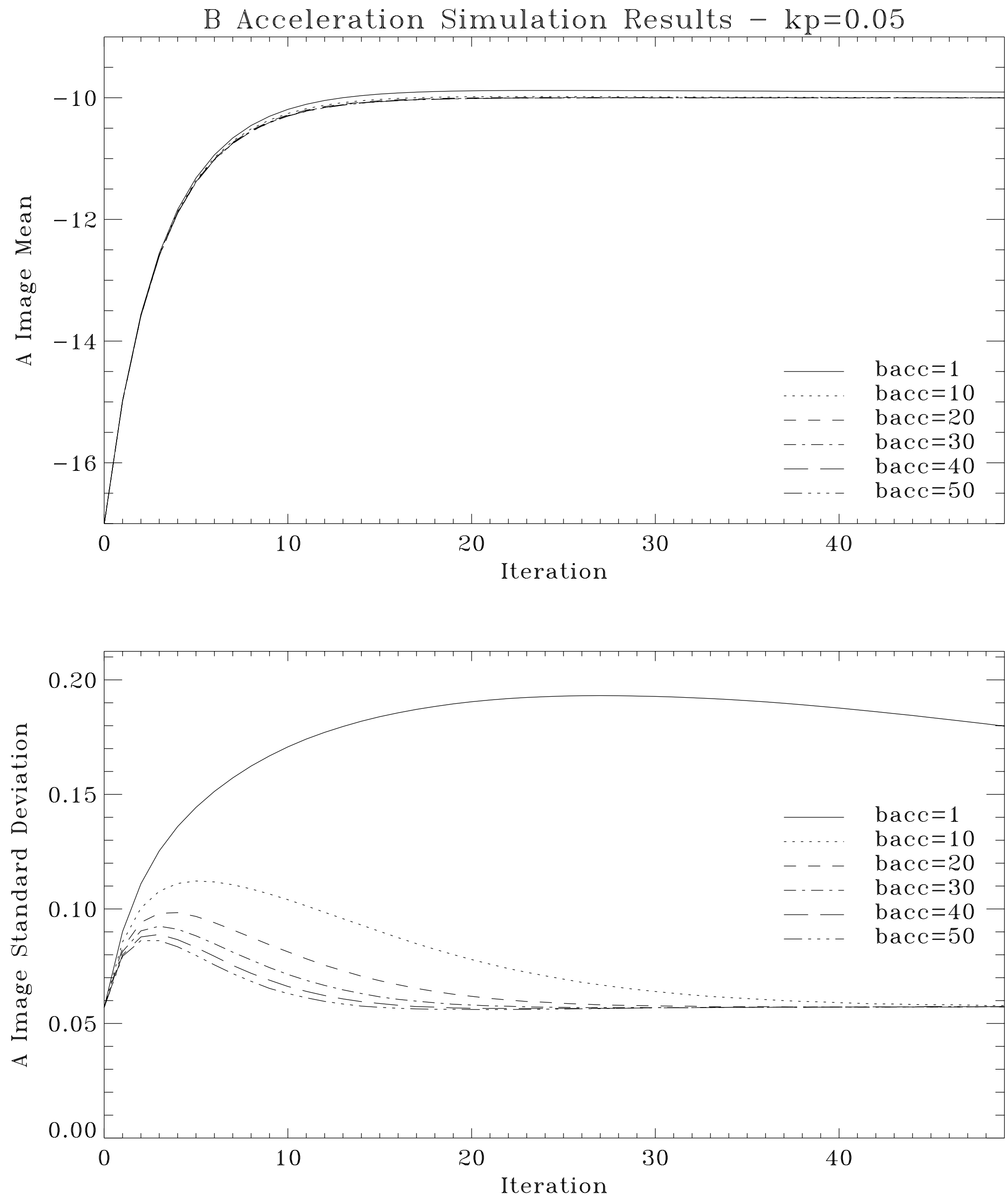

Figure 6: Simulated SIRF $\mathcal{A}$ mean and standard deviations as a function of iteration number and b_{acc} for K_p=0.05.

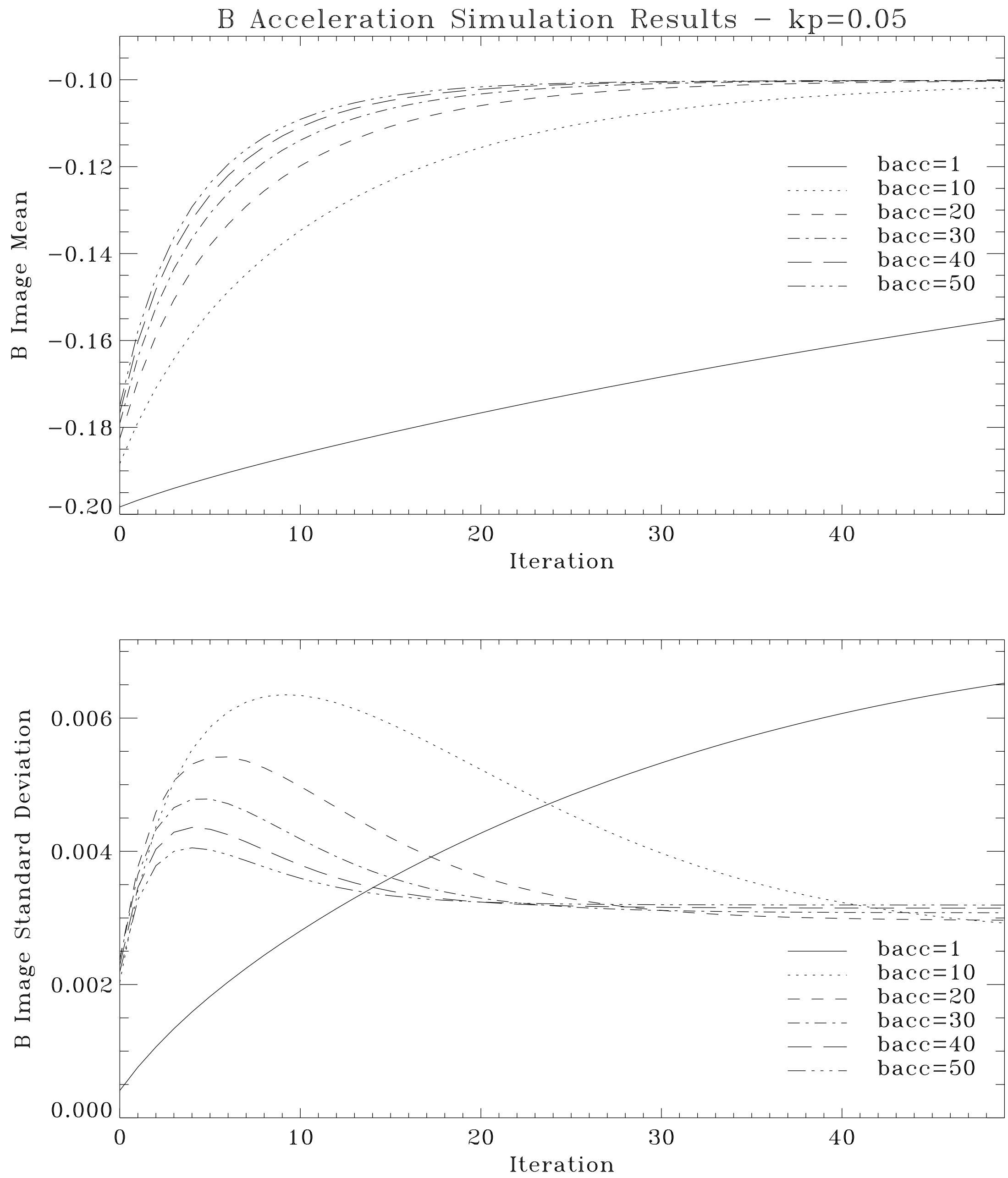

Figure 7: Simulated SIRF $\mathcal{B}$ mean and standard deviations as a function of iteration number and b_{acc} for K_p=0.05.

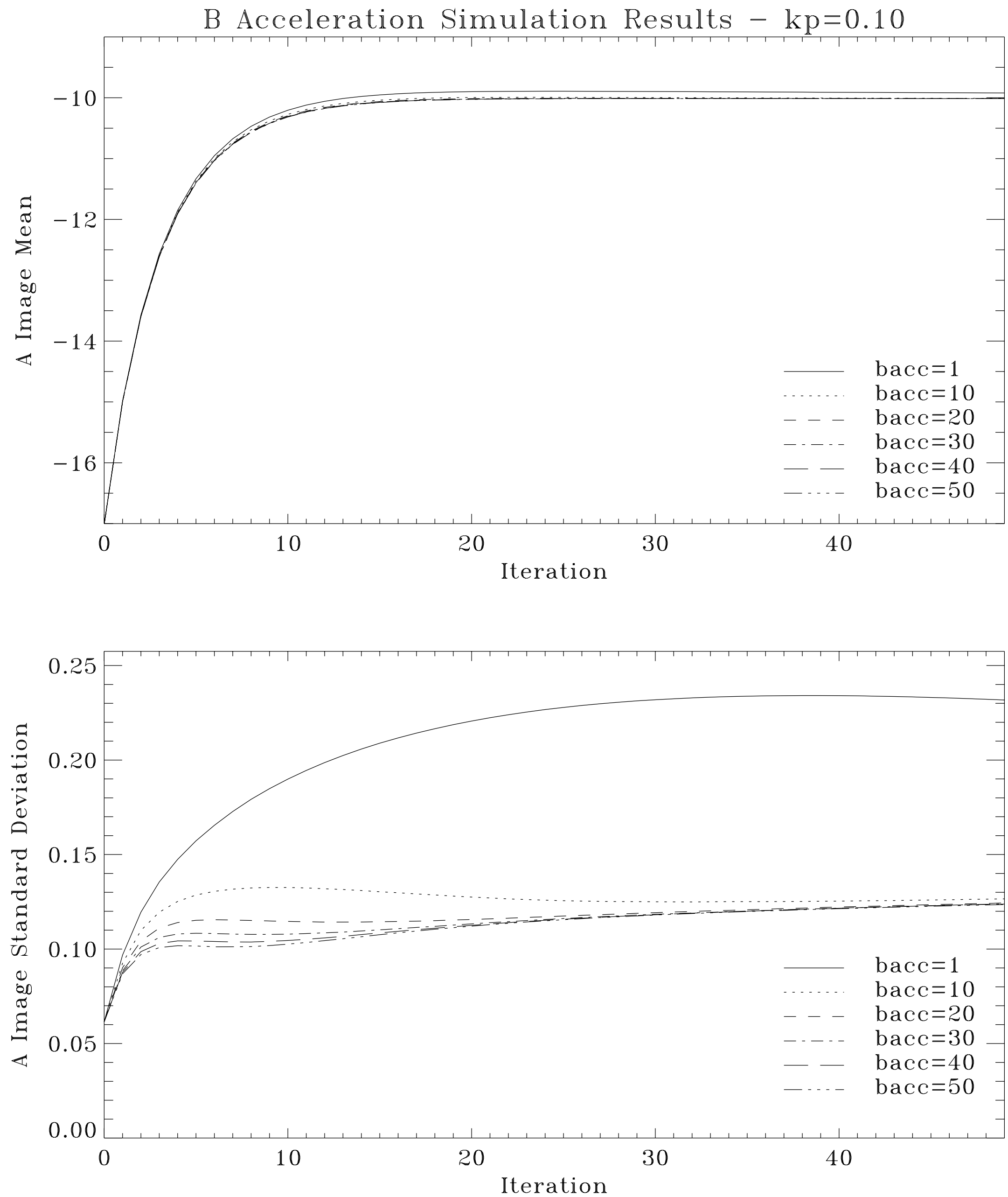

Figure 8: Simulated SIRF $\mathcal{A}$ mean and standard deviations as a function of iteration number and b_{acc} for K_p=0.10.

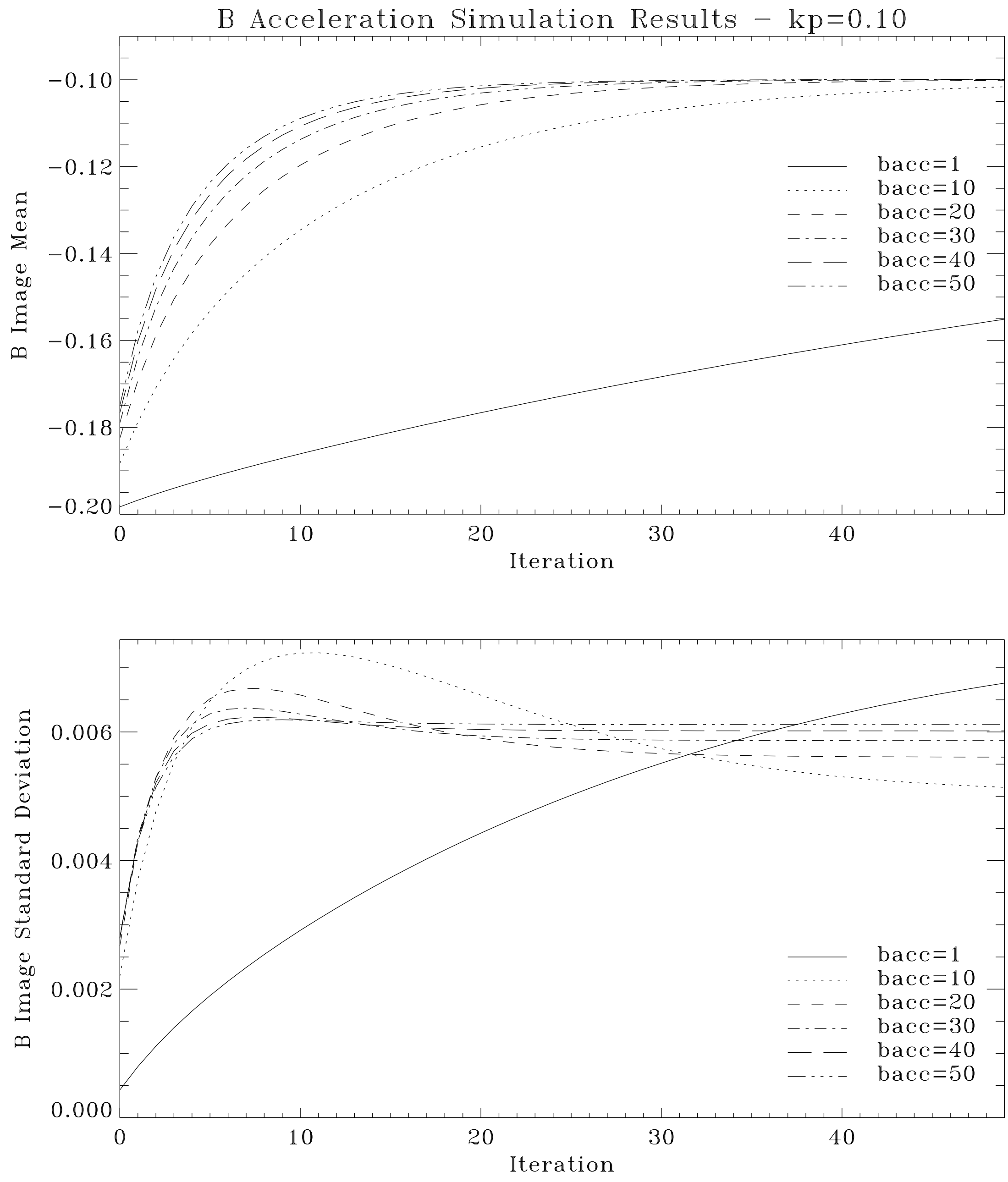

Figure 9: Simulated SIRF $\mathcal{B}$ mean and standard deviations as a function of iteration number and b_{acc} for K_p=0.10.

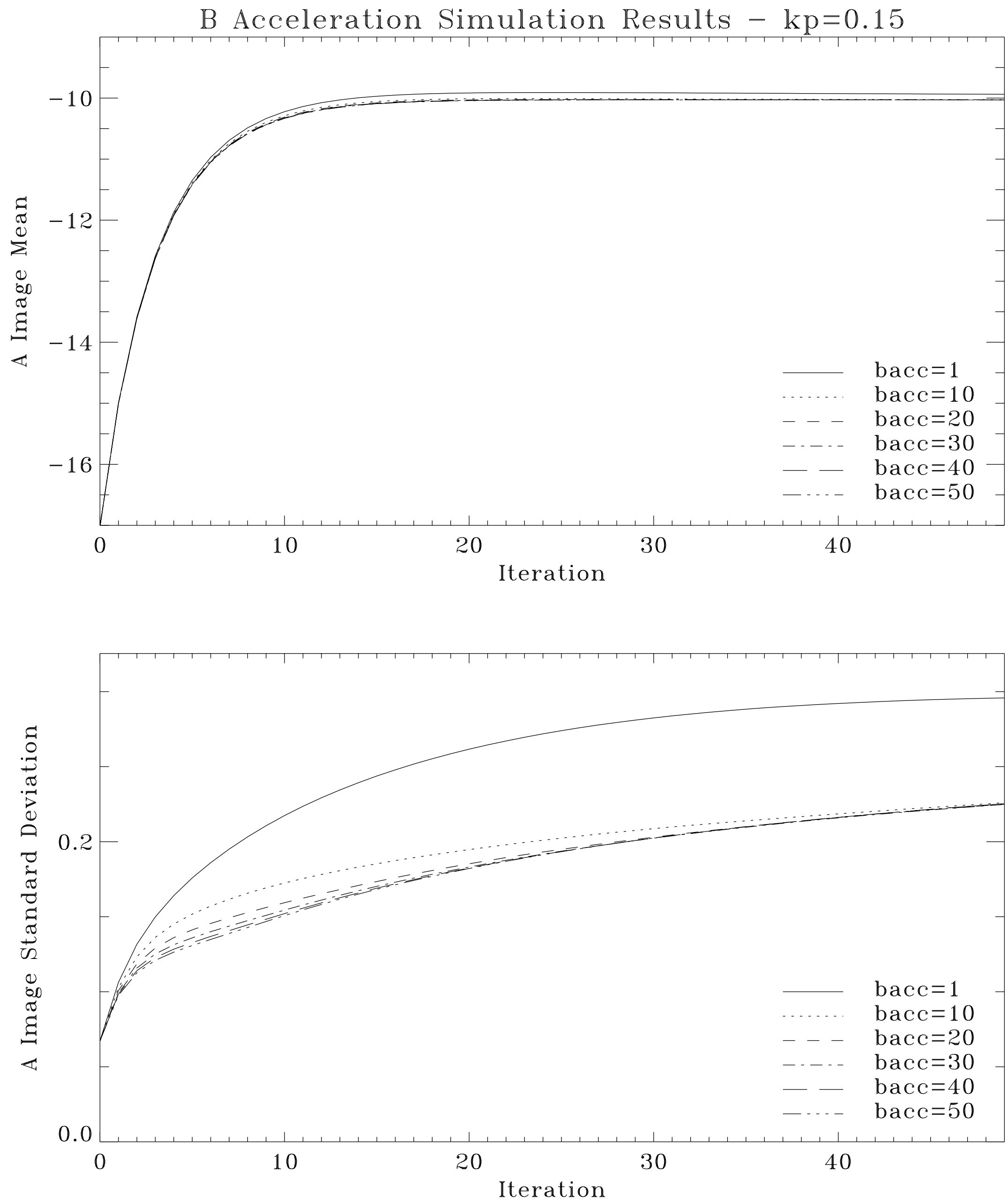

Figure 10: Simulated SIRF $\mathcal{A}$ mean and standard deviations as a function of iteration number and b_{acc} for K_p=0.15.

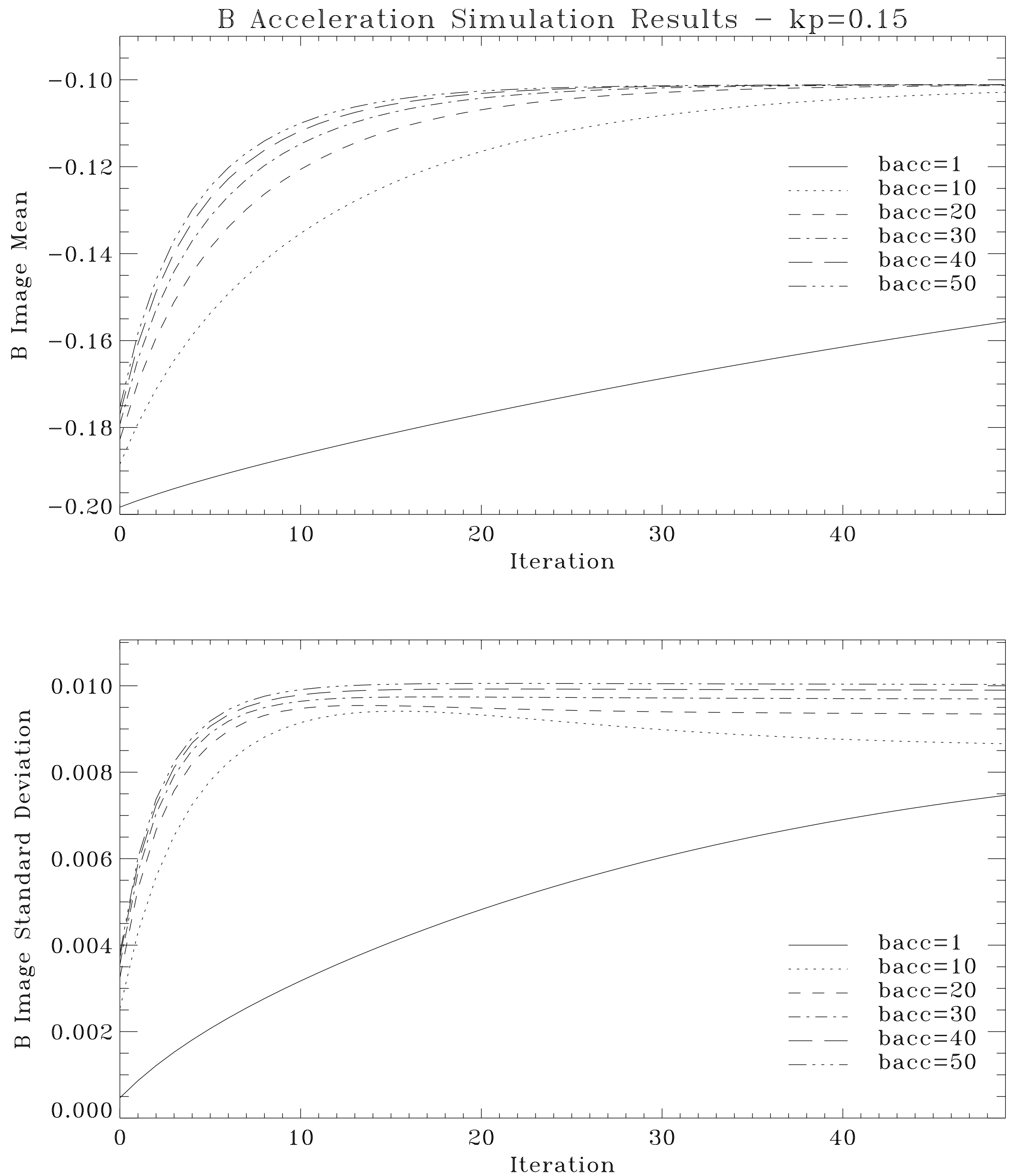

Figure 11: Simulated SIRF $\mathcal{B}$ mean and standard deviations as a function of iteration number and b_{acc} for K_p=0.15.

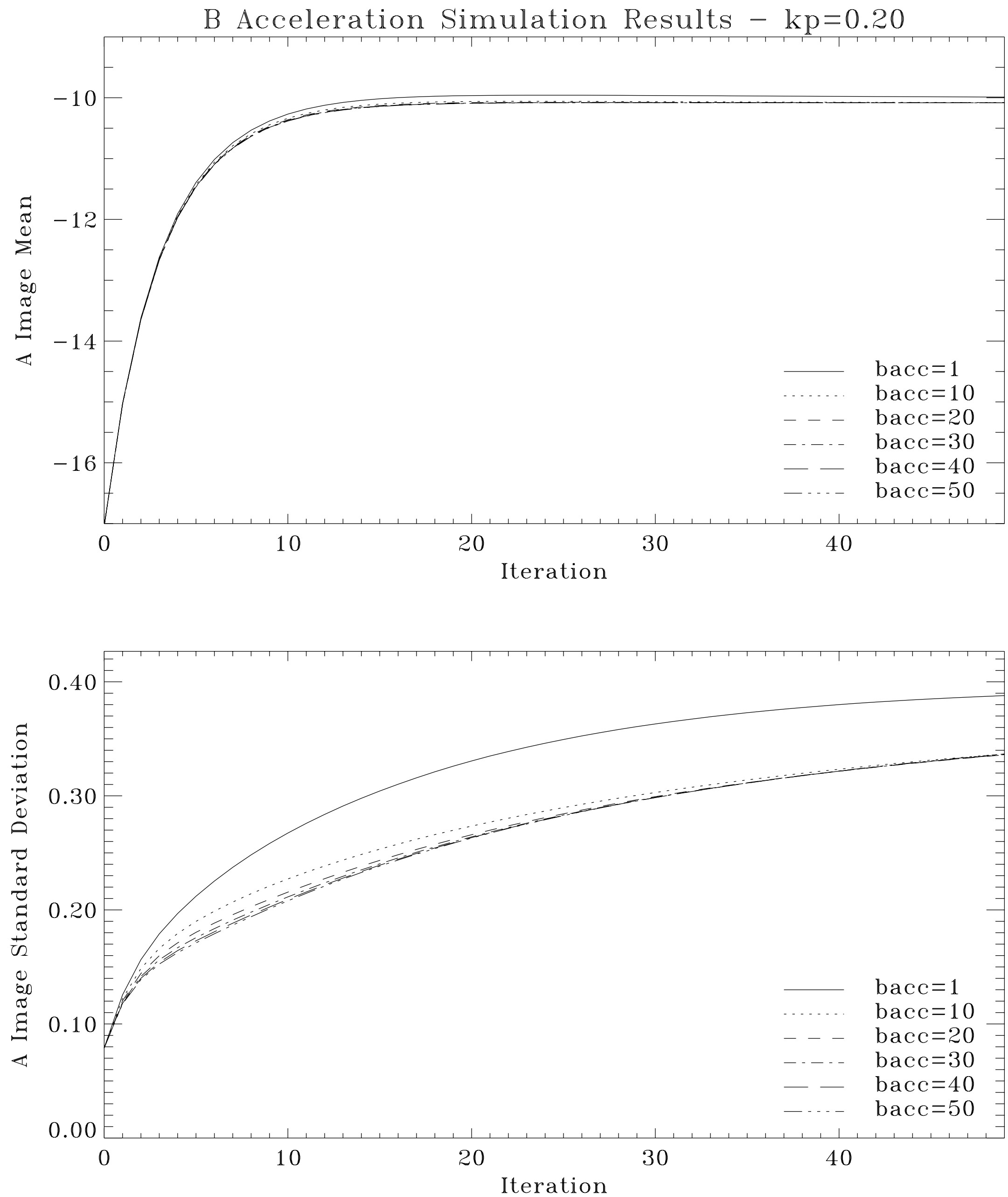

Figure 12: Simulated SIRF $\mathcal{A}$ mean and standard deviations as a function of iteration number and b_{acc} for K_p=0.20.

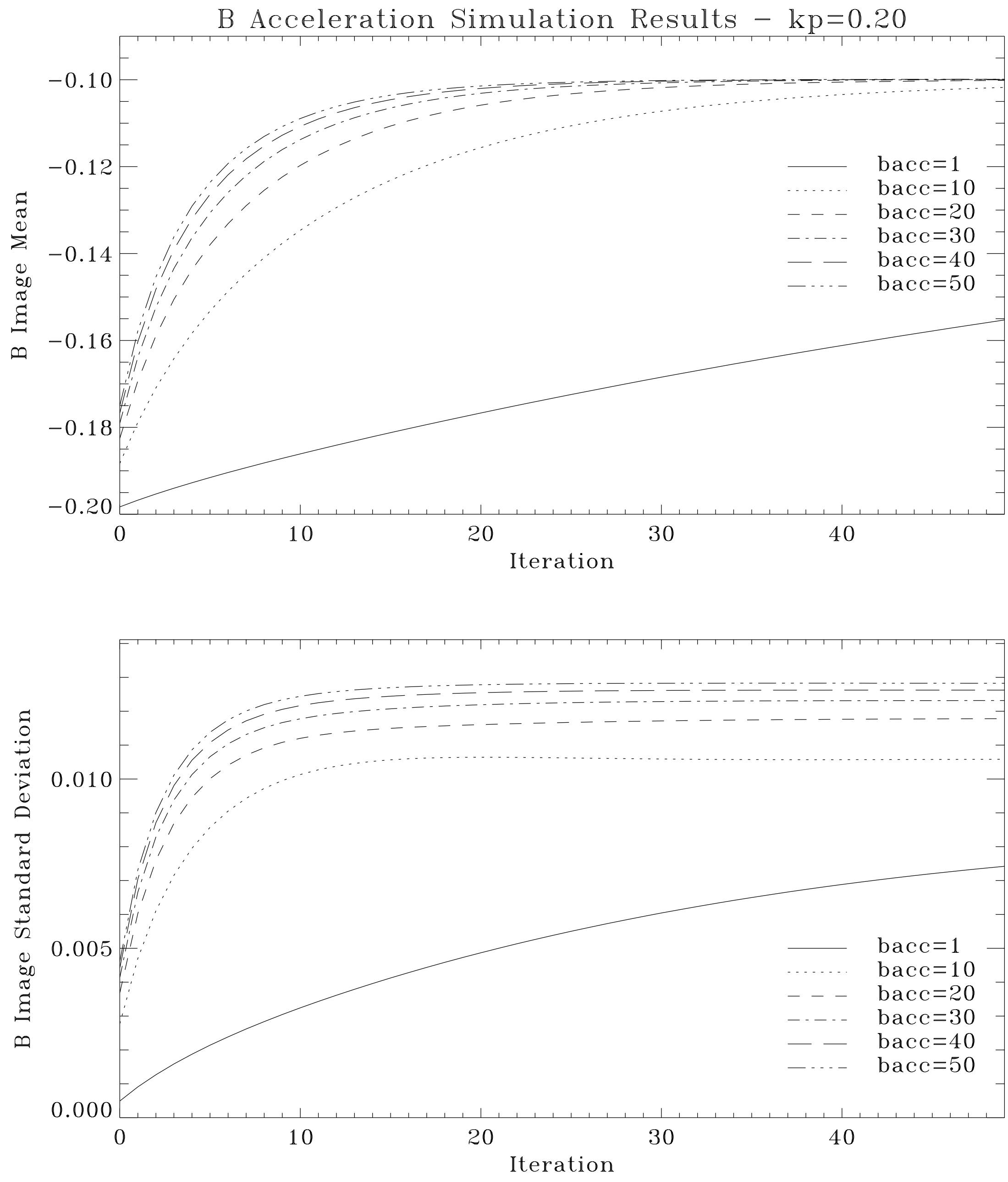

Figure 13: Simulated SIRF $\mathcal{B}$ mean and standard deviations as a function of iteration number and b_{acc} for K_p=0.20.

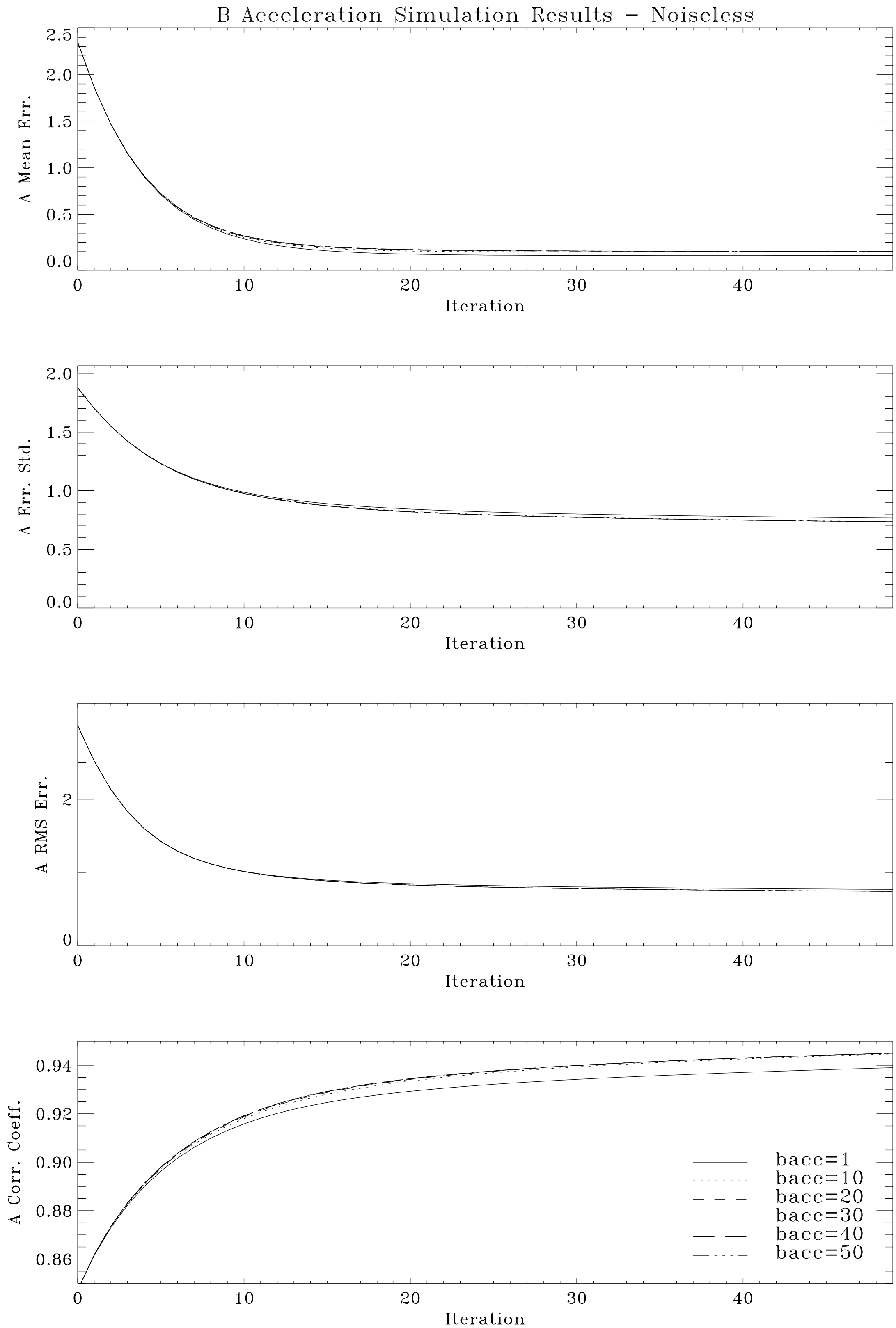

Figure 14: Simulated SIRF $\mathcal{A}$ error and correlation statistics as a function of iteration number and b_{acc} for K_p=0.0.

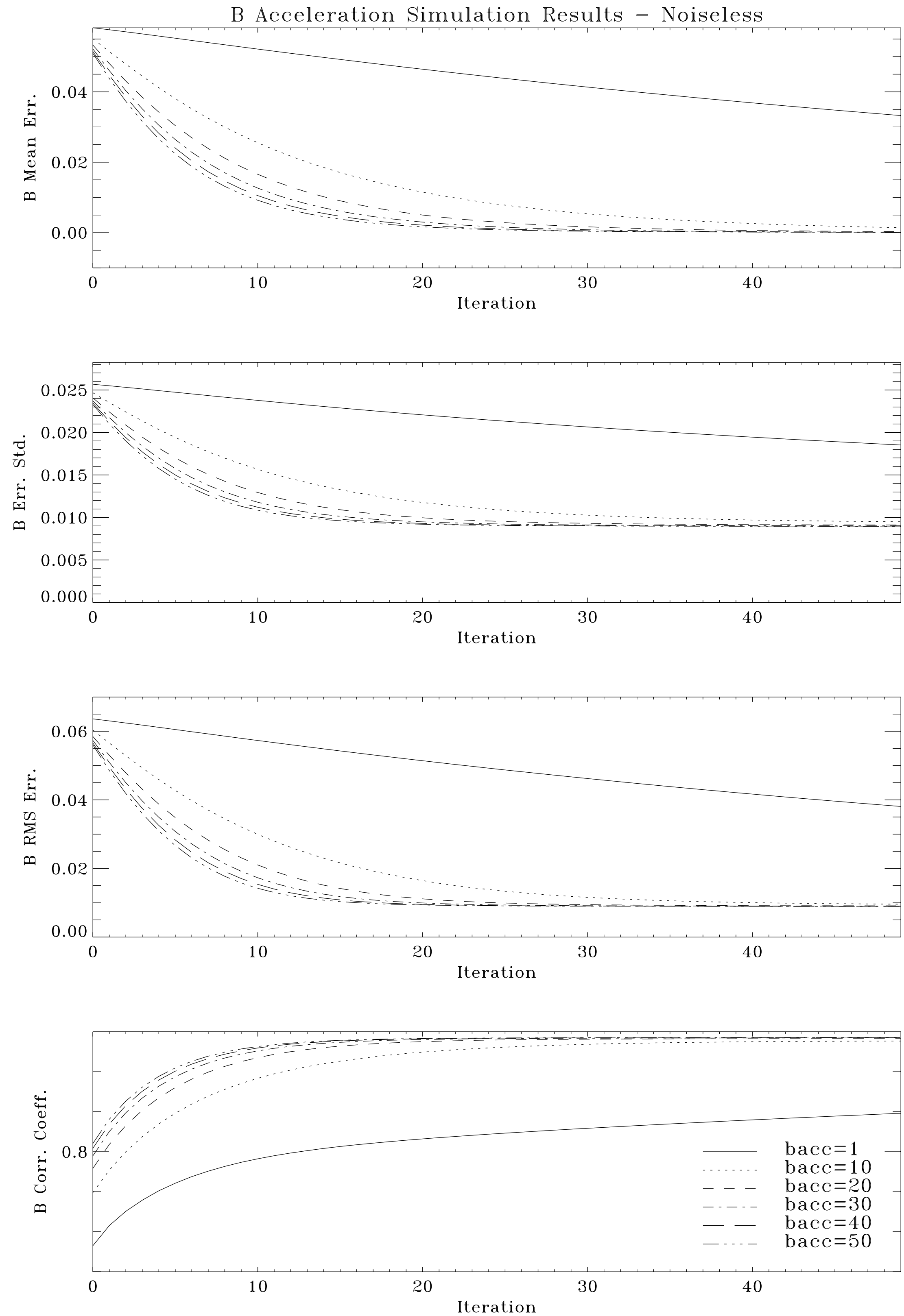

Figure 15: Simulated SIRF $\mathcal{B}$ error and correlation statistics as a function of iteration number and b_{acc} for K_p=0.0.

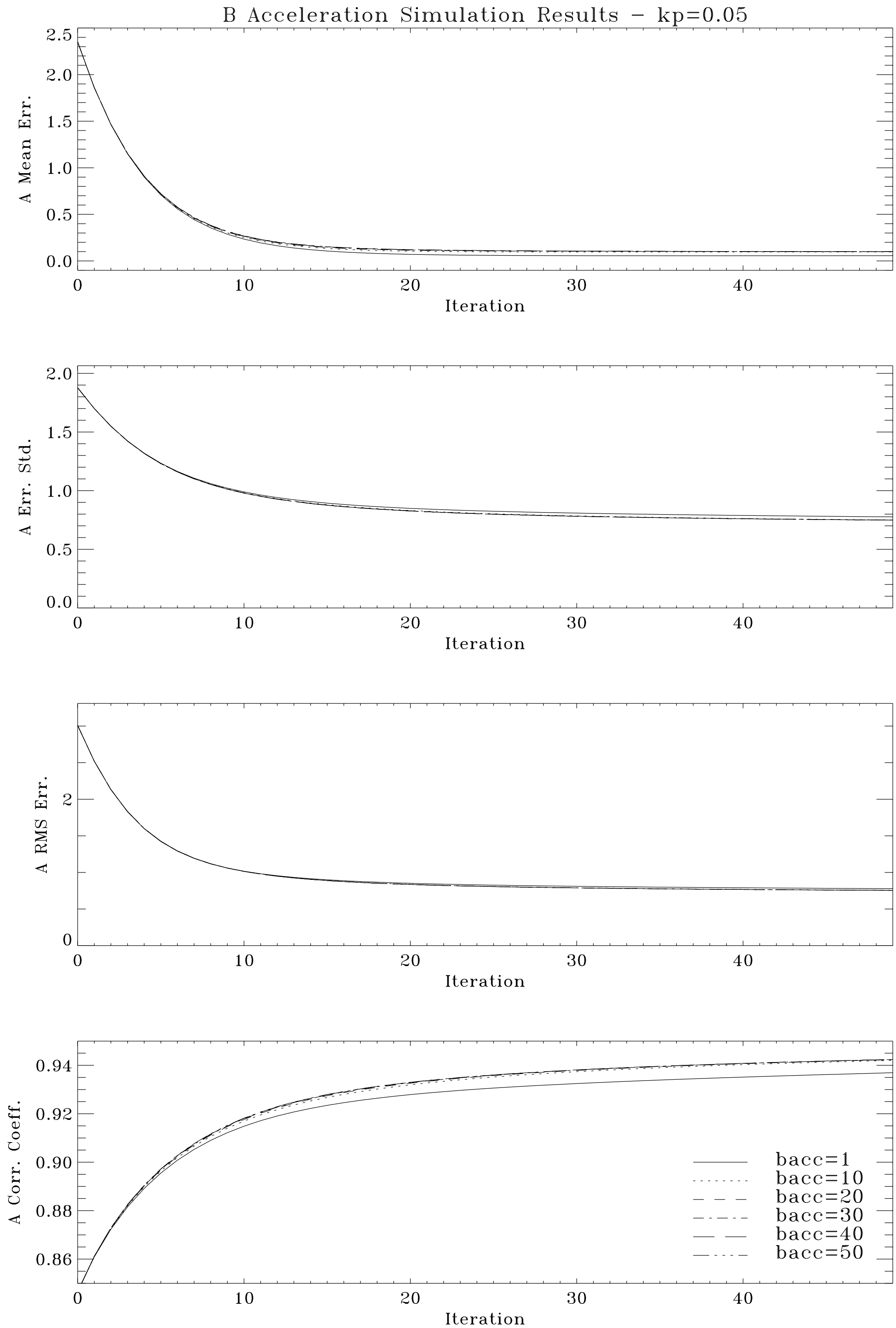

Figure 16: Simulated SIRF $\mathcal{A}$ error and correlation statistics as a function of iteration number and b_{acc} for K_p=0.05.

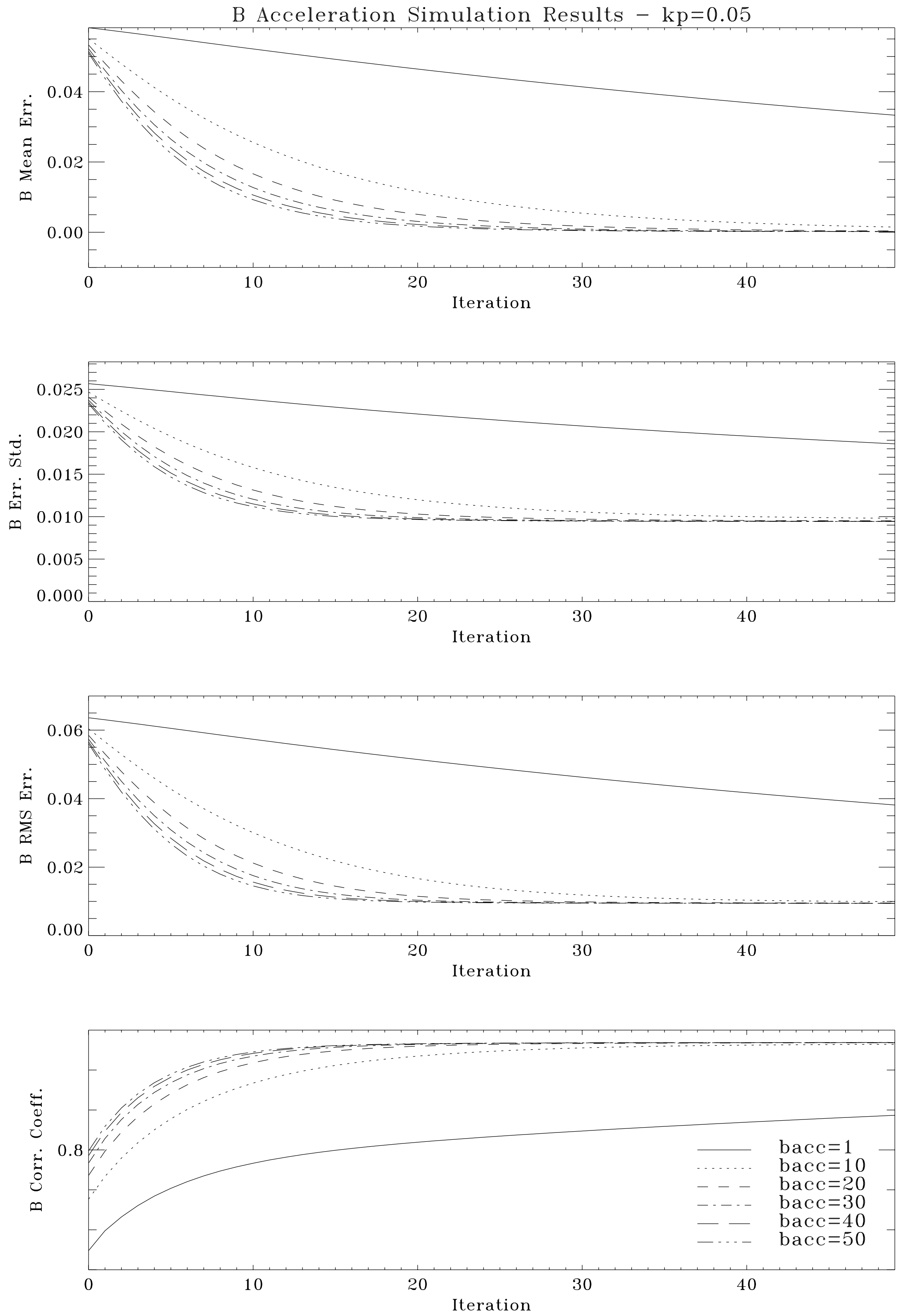

Figure 17: Simulated SIRF $\mathcal{B}$ error and correlation statistics as a function of iteration number and b_{acc} for K_p=0.05.

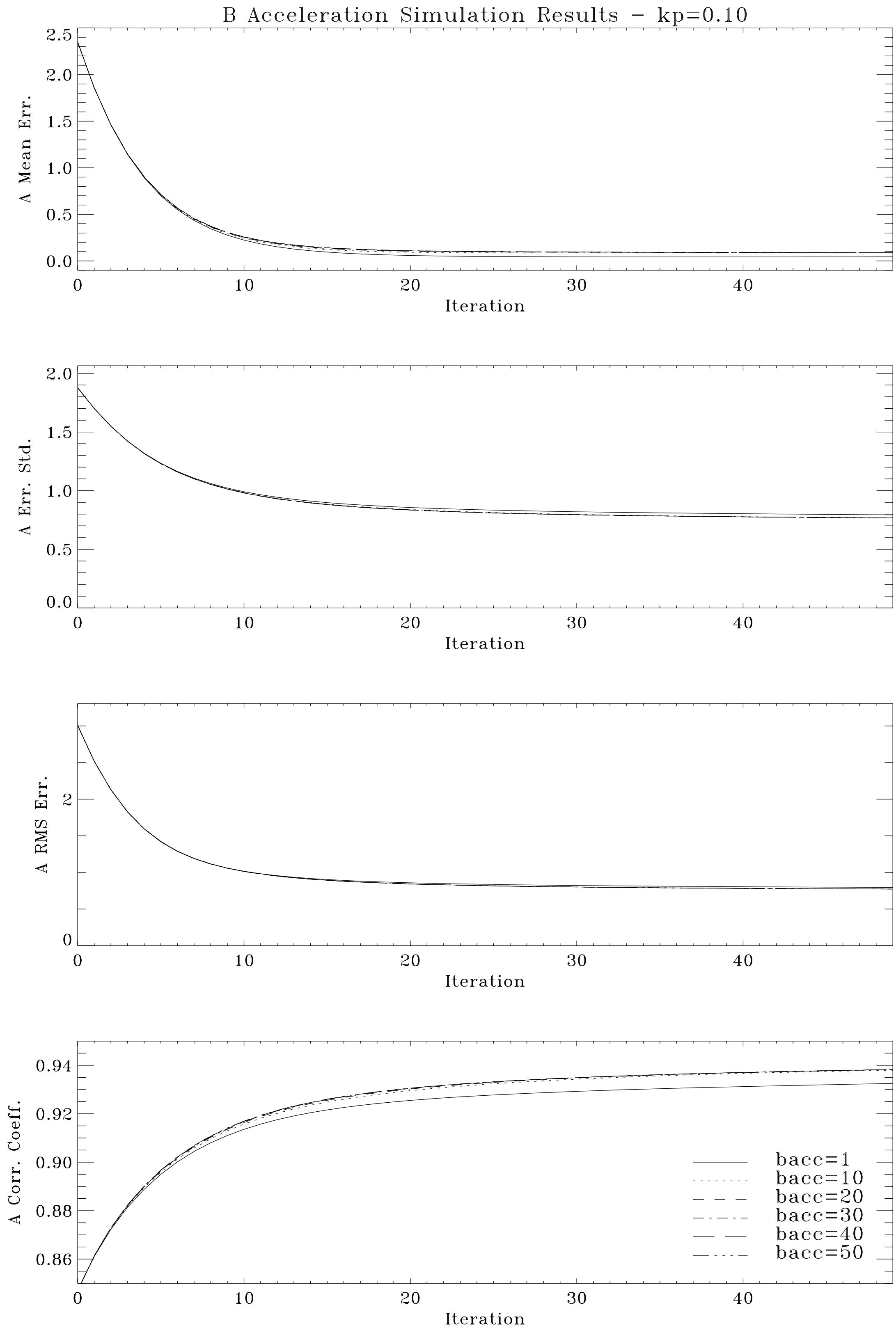

Figure 18: Simulated SIRF $\mathcal{A}$ error and correlation statistics as a function of iteration number and b_{acc} for K_p=0.10.

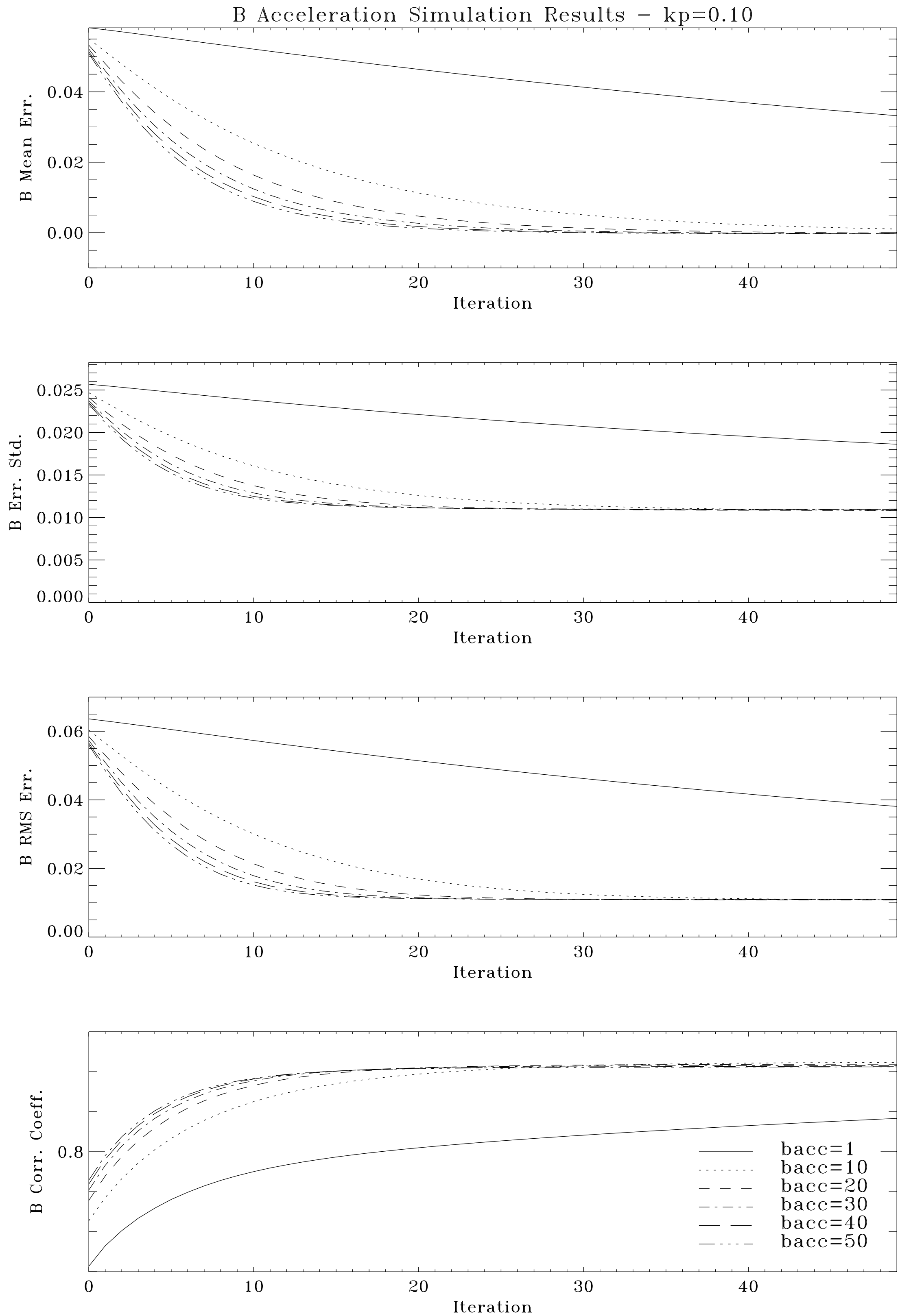

Figure 19: Simulated SIRF $\mathcal{B}$ error and correlation statistics as a function of iteration number and b_{acc} for K_p=0.10.

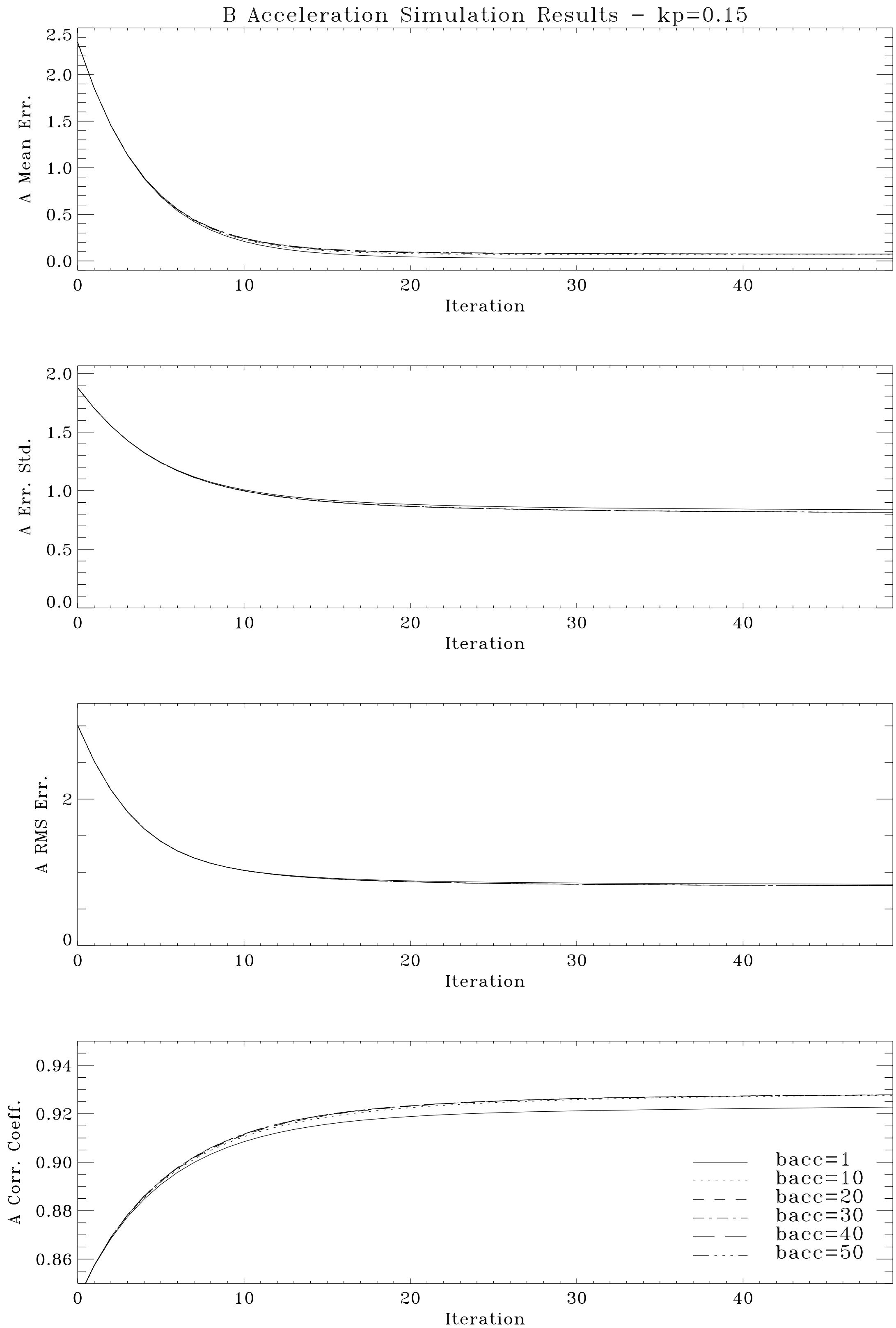

Figure 20: Simulated SIRF $\mathcal{A}$ error and correlation statistics as a function of iteration number and b_{acc} for K_p=0.15.

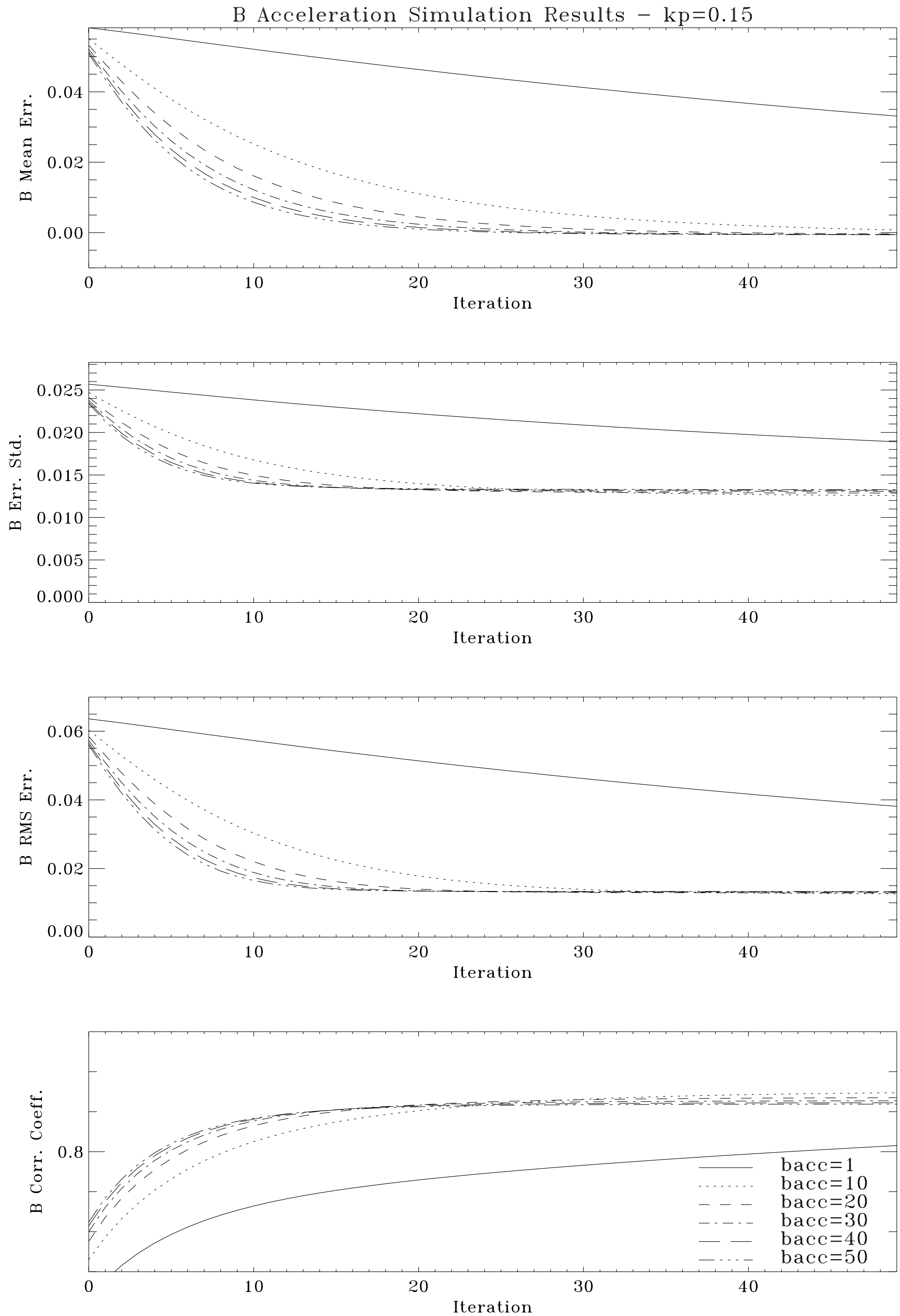

Figure 21: Simulated SIRF $\mathcal{B}$ error and correlation statistics as a function of iteration number and b_{acc} for K_p=0.15.

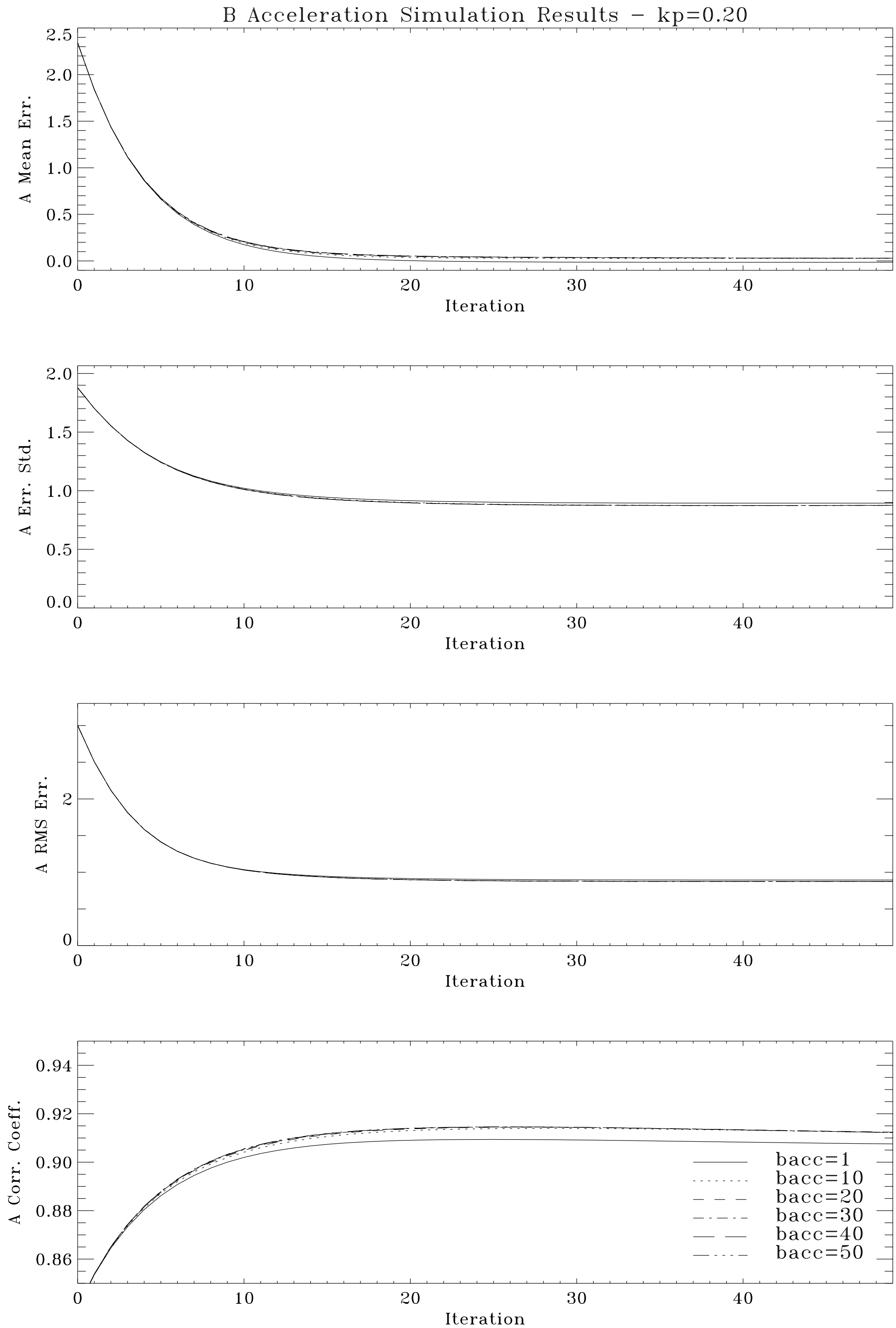

Figure 22: Simulated SIRF $\mathcal{A}$ error and correlation statistics as a function of iteration number and b_{acc} for K_p=0.20.

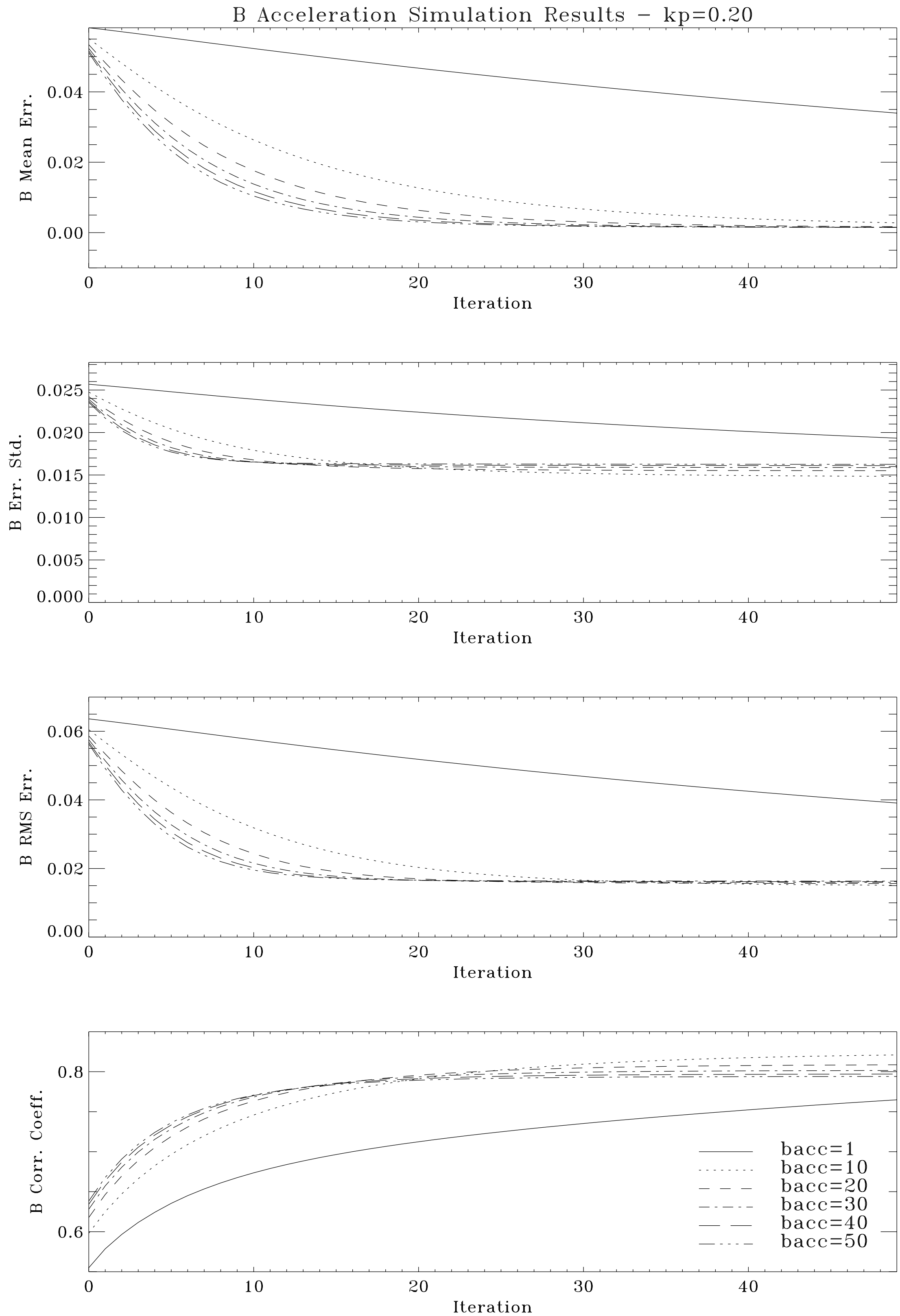

Figure 23: Simulated SIRF $\mathcal{B}$ error and correlation statistics as a function of iteration number and b_{acc} for K_p=0.20.

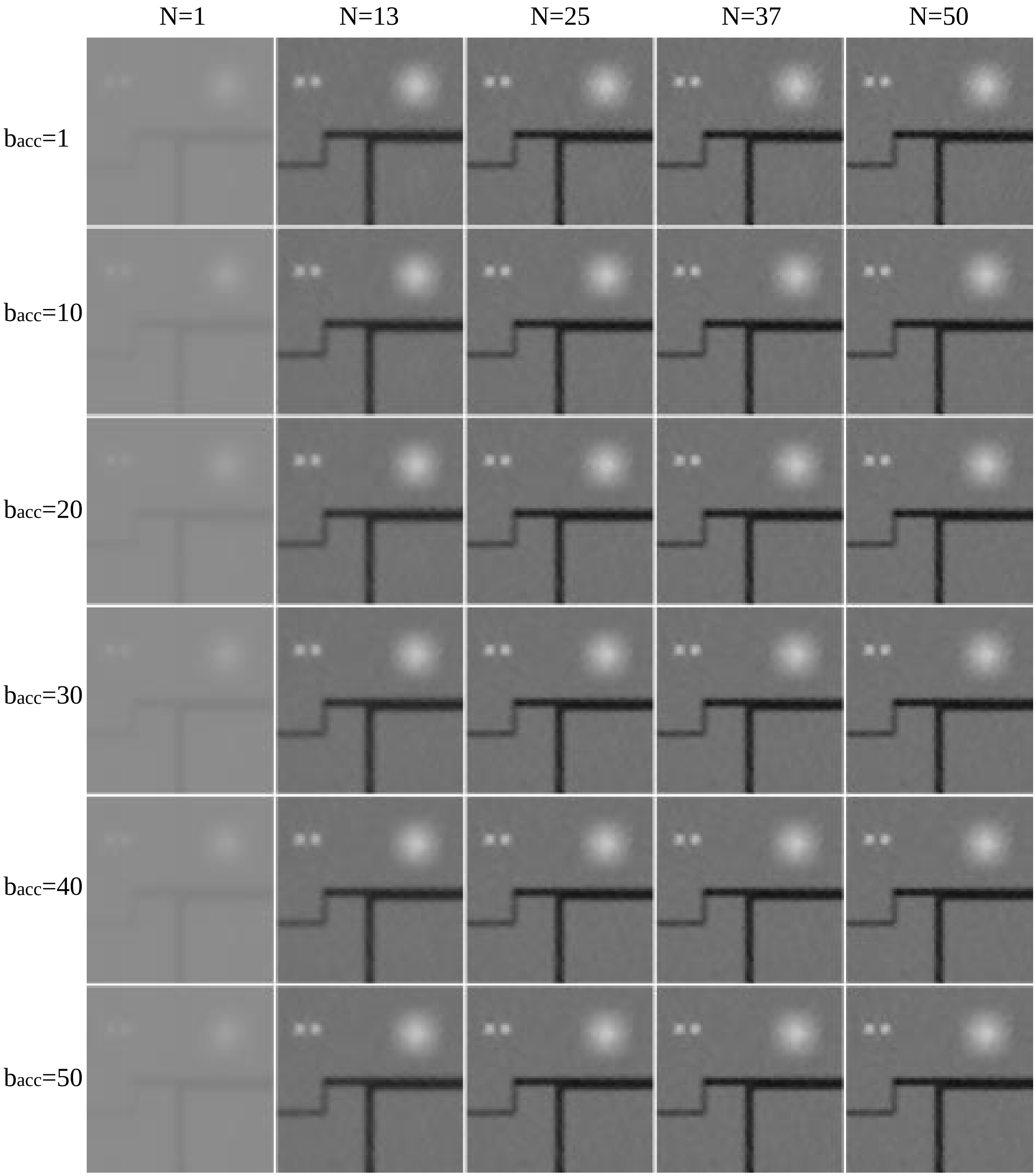

Figure 24: SIRF $\mathcal{A}$ simulation images as a function of iteration number and b_{acc}. K_p=0.10 for all images.

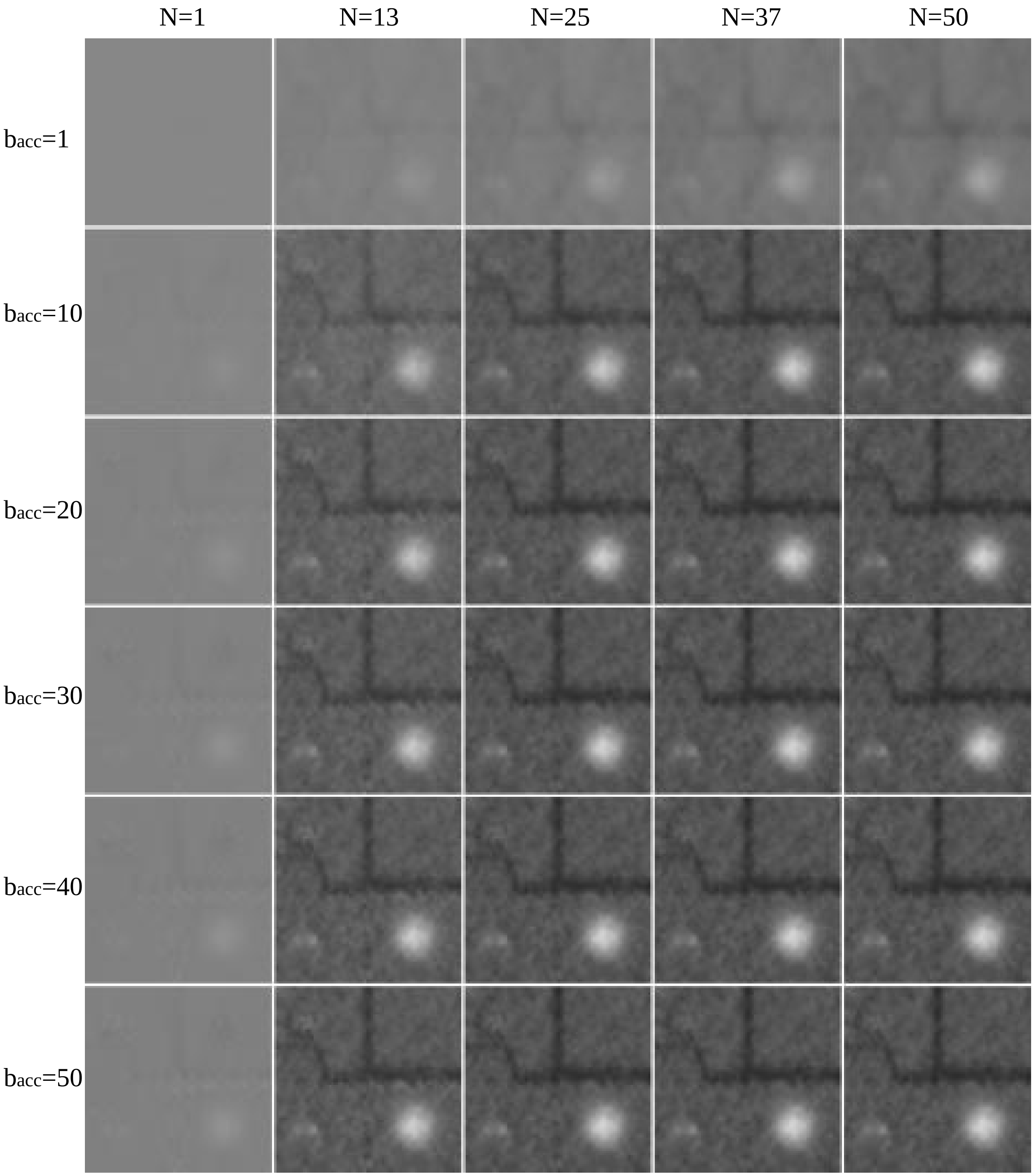

Figure 25: SIRF $\mathcal{B}$ simulation images as a function of iteration number and b_{acc}. K_p=0.10 for all images.

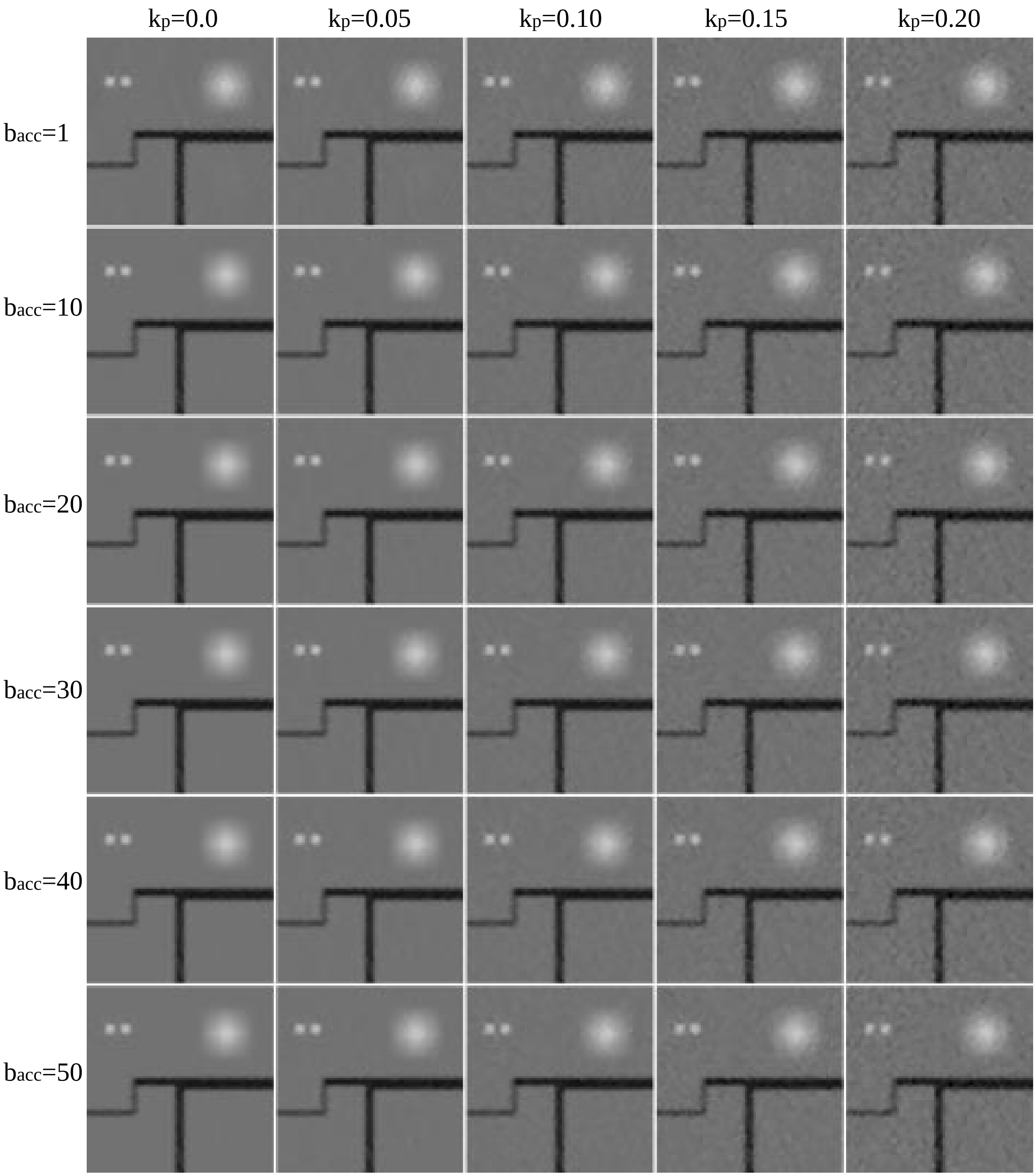

Figure 26: SIRF $\mathcal{A}$ simulation images as a function of K_p and b_{acc}. 50 iterations were used for all images.

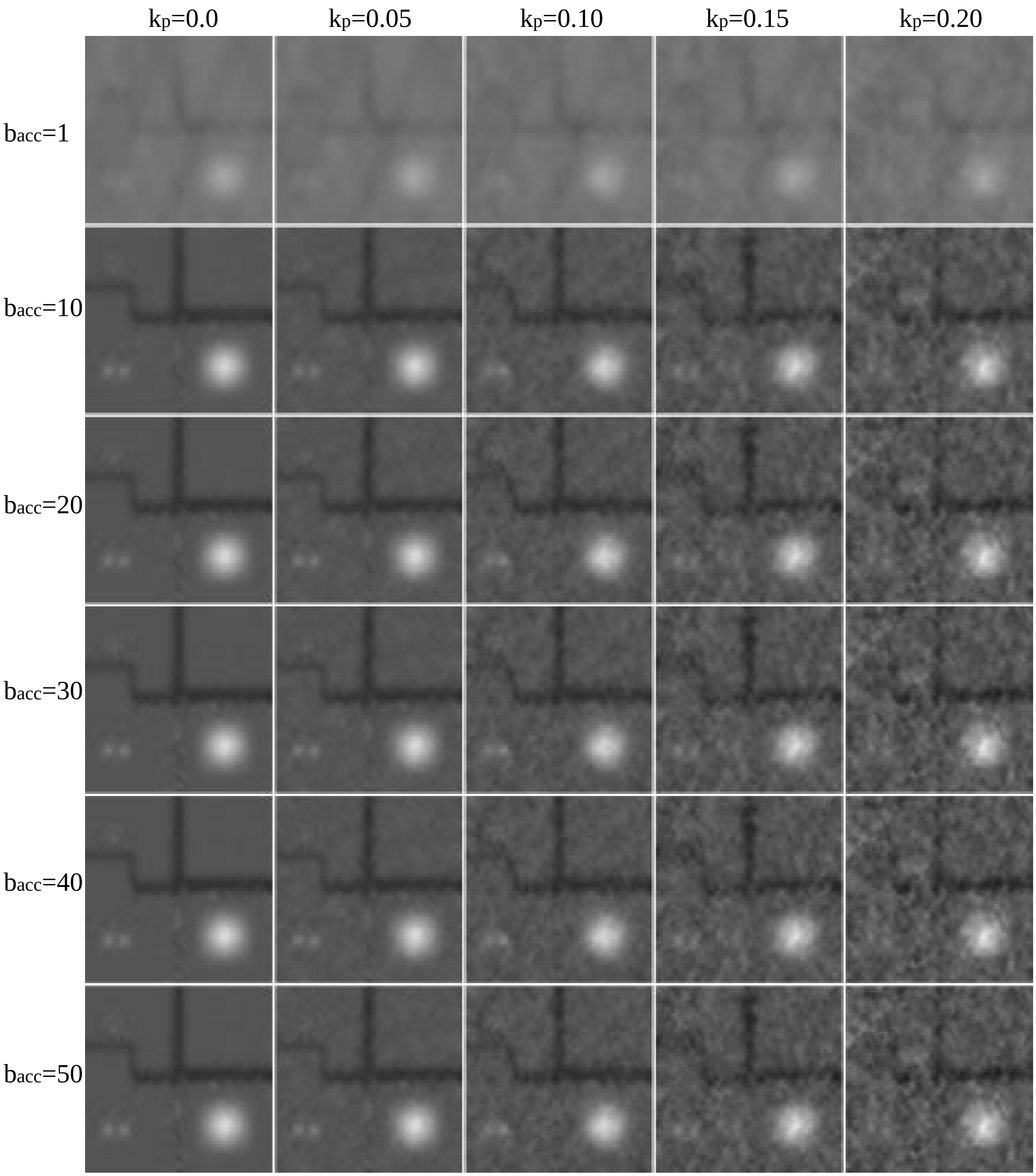

Figure 27: SIRF $\mathcal{B}$ simulation images as a function of K_p and b_{acc}. 50 iterations were used for all images.

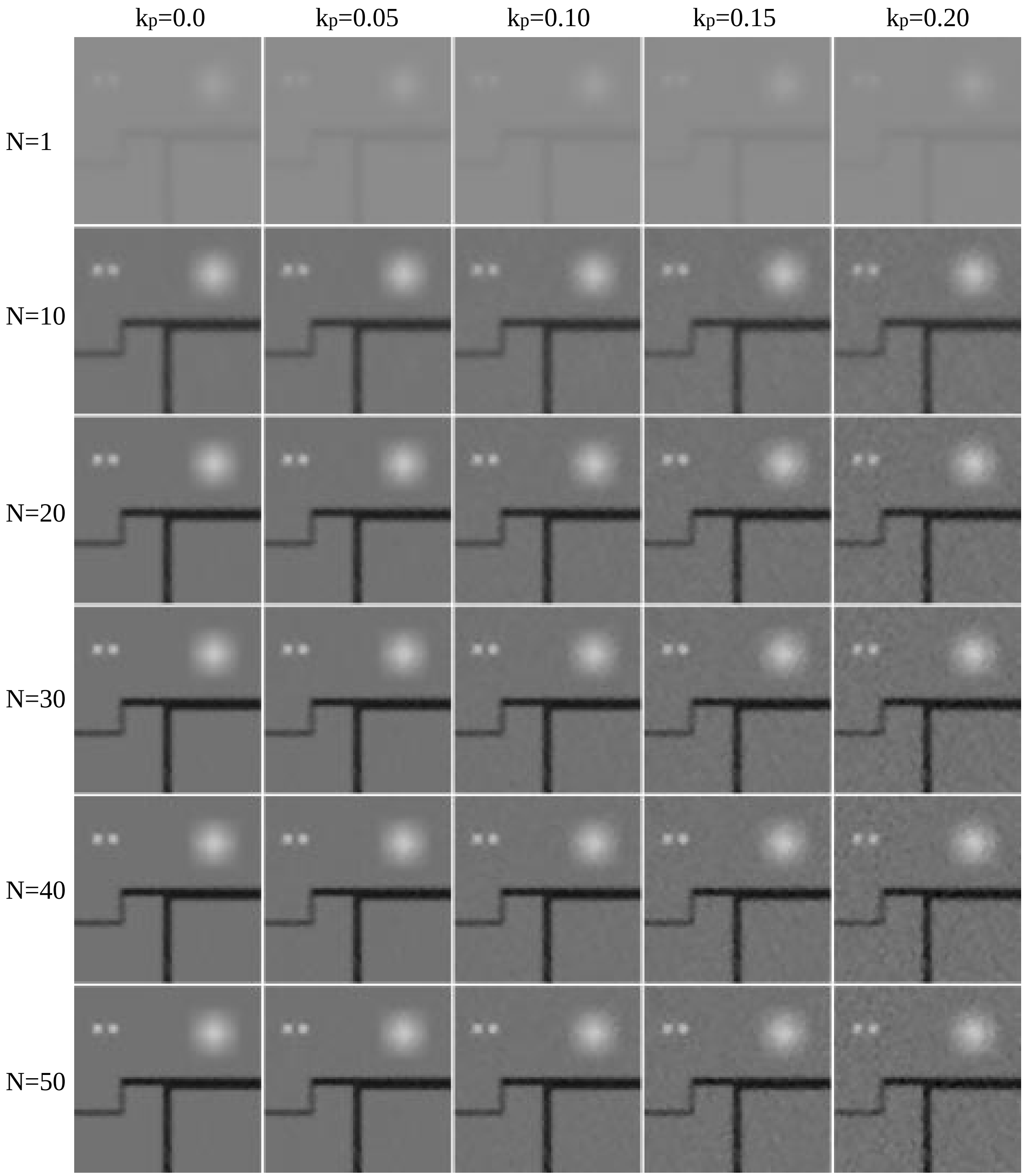

Figure 28: SIRF $\mathcal{A}$ simulation images as a function of K_p and iteration number. b_{acc}=30 for all images.

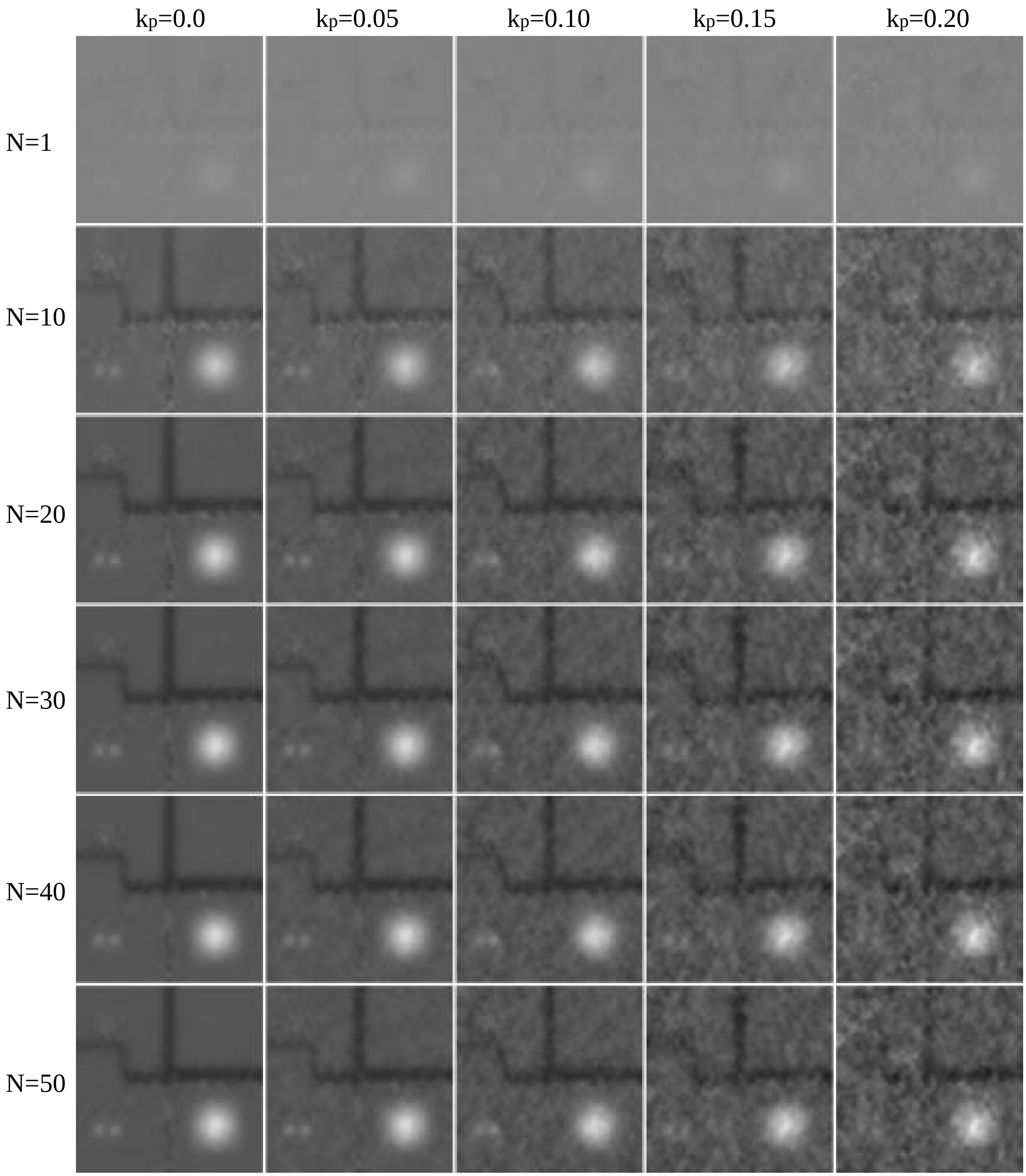

Figure 29: SIRF $\mathcal{B}$ simulation images as a function of K_p and iteration number. b_{acc}=30 for all images.